Journal of Advanced Research 73 (2025) 357–373

Contents lists available at ScienceDirect

Journal of Advanced Research

journal homepage: www.elsevier.com/locate/jare

CDK4/6 inhibitor PD-0332991 suppresses hepatocarcinogenesis by inducing senescence of hepatic tumor-initiating cells

Miaomiao Chen [a,b,c,1], Wenjian Chen [a,b,c,1], Shiwen Sun [a,b,c,1], Yanli Lu [a,b,c], Guoxiu Wu [a,b,c], Hongyu Xu [a,b,c], Huiru Yang [a,b,c], Chong Li [d], Weizhi He [a,b,c], Mingyang Xu [a,b,c], Xiuhua Li [a,b,c], Dong Jiang [a,b,c], Yongchao Cai [a,b,c], Changcheng Liu [a,b,c], Wencheng Zhang [a,b,c], Zhiying He [a,b,c,*]

[a] *Institute for Regenerative Medicine, Medical Innovation Center and State Key Laboratory of Cardiology, Shanghai East Hospital, School of Life Sciences and Technology, Tongji University, Shanghai 200123, P. R. China*
[b] *Shanghai Engineering Research Center of Stem Cells Translational Medicine, Shanghai 200335, P. R. China*
[c] *Shanghai Institute of Stem Cell Research and Clinical Translation, Shanghai 200120, P. R. China*
[d] *Zhoupu Community Health Service Center of Pudong New Area, Shanghai, China*

HIGHLIGHTS

- Treatment with PD-0332991 during the pre-cancerous stage significantly reduced the incidence of HCC in two mouse models.
- The administration of PD-0332991 induced senescence in hTICs and interrupted the development of hTICs into HCC.
- The "CyclinD-CDK4/6-INK4-Rb" pathway activated during the pre-HCC stage and PD-0332991 inhibited this pathway.
- The senescent hTICs expressed CCL2 and CXCL10, which recruited and activated macrophages, enhanced anti-tumor immunity.

GRAPHICAL ABSTRACT

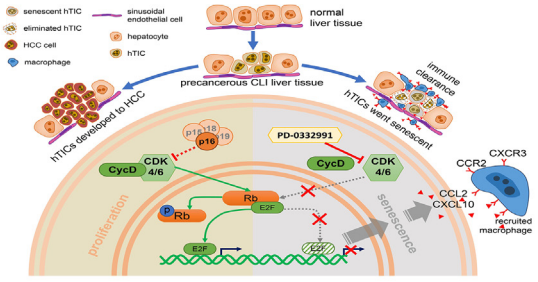

ARTICLE INFO

Article history:
Received 8 April 2024
Revised 8 August 2024
Accepted 26 August 2024
Available online 31 August 2024

Keywords:
HCC
CDK4/6 inhibitors
Tumor-initiating cells
Cellular senescence
Cyclin D-CDK4/6-INK4-Rb pathway

ABSTRACT

Introduction: Owing to the limited treatment options for hepatocellular carcinoma (HCC), interventions targeting pre-HCC stages have attracted increasing attention. In the pre-HCC stage, hepatic tumor-initiating cells (hTICs) proliferate abnormally and contribute to hepatocarcinogenesis. Numerous studies have investigated targeted senescence induction as an HCC intervention. However, it remains to be clarified whether senescence induction of hTICs could serve as a pre-HCC intervention.
Objectives: This study was designed to investigate whether senescence induction of hTICs in the precancerous stage inhibit HCC initiation.
Methods and Results: HCC models developed from chronic liver injury (CLI) were established by using *Fah*$^{-/-}$ mice and N-Ras + AKT mice. PD-0332991, a selective CDK4/6 inhibitor that blocks the G1/S transition in proliferating cells, was used to induce senescence during the pre-HCC stage. Upon administration of PD-0332991, we observed a significant reduction in HCC incidence following selective senescence induction in hTICs, and an alleviation liver injury in the CLI-HCC models. PD-0332991 also induced

* Corresponding author at: Institute for Regenerative Medicine, Medical Innovation Center and State Key Laboratory of Cardiology, Shanghai East Hospital, School of Life Sciences and Technology, Tongji University, Shanghai 200123, P. R. China.
E-mail address: zyhe@tongji.edu.cn (Z. He).
[1] **These authors contributed equally to this work.**

https://doi.org/10.1016/j.jare.2024.08.034

senescence *in vitro* in cultured hTICs isolated from CLI-HCC models. Moreover, RNA sequencing (RNA-seq) analysis delineated that the "Cyclin D-CDK4/6-INK4-Rb" pathway was activated in both mouse and human liver samples during the pre-HCC stage, while PD-0332991 exhibited substantial inhibition of this pathway, thereby inducing cellular senescence in hTICs. Regarding the immune microenvironment, we demonstrated that senescent hTICs secrete key senescence-associated secretory phenotypic (SASP) factors, CXCL10 and CCL2, to activate and recruit macrophages, and contribute to immune surveillance.
Conclusion: We found that hTICs can be targeted and induced into a senescent state during the pre-HCC stage. The SASP factors released by senescent hTICs further activate the immune response, facilitating the clearance of hTICs, and consequently suppressing HCC occurrence. We highlight the importance of pre-HCC interventions and propose that senescence-inducing drugs hold promise for preventing HCC initiation under CLI.

Introduction

Primary liver cancer is the third leading cause of cancer-related mortality worldwide [1]. Hepatocellular carcinoma (HCC) accounts for approximately 75 %-85 % of primary liver cancers and has a poor prognosis owing to limited anti-cancer drugs and a low objective remission rate. Generally, HCC is the outcome of long-term progression of many diseases associated with chronic liver injuries (CLI). A long-term progression before HCC formation offers promising opportunities for early intervention [2,3]. Tumor initiation is orchestrated by a group of malignant cells capable of long-term tumorigenicity known as tumor-initiating cells (TICs) [4]. In the liver, hepatic TICs (hTICs) are also involved in HCC initiation [5,6]. Hence, targeting TICs would be a promising approach for reducing the tumorigenic potential of CLI.

As a useful intrinsic and effective antitumor strategy, cellular senescence is a condition in which cells permanently exit the cell cycle and cease to proliferate [7,8]. Hepatocytes overexpressing *RAS* rapidly undergo oncogene-induced senescence, which is accompanied by senescence-associated secretory phenotype (SASP) factors that activate the immune response, thereby inhibiting HCC [9]. Another study revealed that the cell cycle inhibitor XL413 specifically induces senescence in p53-mutant HCC cells and slows HCC progression [10], suggesting that cellular senescence induction is a promising strategy for delaying the development of HCC. Thus, it is crucial to investigate whether senescence induction of hTICs could prevent hepatocarcinogenesis and serve as a potential strategy for cancer prevention and treatment.

Cyclin-dependent kinases 4 and 6 (CDK4/6) and the Cyclin D-CDK4/6-INK4-Rb pathway, in which CDK4/6 are components, play central roles in cell cycle regulation. The inhibition of CDK4/6 causes cell cycle arrest and induces cellular senescence [11,12]. Aberrant activation of this pathway accelerates the G1 phase and G1/S transition, and promotes cell proliferation. Among human tumors with normal Rb protein function, 80 % harbor abnormalities in the Cyclin D-CDK4/6-Rb pathway, mainly characterized by *CDKN2A* inactivation, *CDK4* amplification, or *CCND1* overexpression [13]. Over-activation of Cyclin D1-CDK4/6 kinases are closely related to the occurrence, progression, and prognosis of various tumors, including HCC, and offers potential therapeutic targets for HCC [14].

PD-0332991, a small-molecule inhibitor of CDK4/6, specifically and competitively inhibits the binding of CDK4/6 to ATP. This inhibition disrupts the formation of CDK4/6-Cyclin D heterodimers, ultimately reducing the phosphorylation of the Rb protein [15,16]. Among susceptible breast cancer cell subtypes, PD-0332991 induced senescence *in vitro*. The US Food and Drug Administration (FDA) has approved PD-0332991 for the clinical treatment of advanced ER^+HER2^- breast cancer [17,18]. In myeloma and lung cancer cells, administration of PD-0332991 blocked the G0/G1 transition and induced the expression of cellular senescence markers. In HCC cell lines with normal Rb protein function, PD-0332991 also induces cellular senescence [15,19,20]. Therefore, PD-0332991 is a well-studied drug for inducing cellular senescence. However, it is uncertain whether PD-0332991 can elicit cellular senescence in hTICs, and whether this induction would achieve preferable efficacy in preventing HCC.

Previously, we explored the relationship between hepatocyte senescence and HCC development using fumarylacetoacetate hydrolase (Fah) knockout ($Fah^{-/-}$) mouse models with different degrees of liver injury [21]. $Fah^{-/-}$ mice suffer acute liver injury due to the accumulation of toxic metabolites, and the production of metabolites can be blocked by therapeutic doses of nitisinone (NTBC) [22,23]; however, under low doses of NTBC administration, small amounts of toxic metabolite production still existed, which could induce CLI and subsequently hepatocarcinogenesis [24,25]. By comparing the senescence pattern and HCC incidence under acute and CLI, we demonstrated that hepatocyte senescence is a major protective mechanism against hepatocarcinogenesis in liver injury, indicating the possibility of inducing hepatocyte senescence to inhibit hepatocarcinogenesis in patients with CLI [21].

In the present study, we investigated the potential application of the CDK4/6 inhibitor, PD-0332991, for pre-HCC intervention based on $Fah^{-/-}$ and N-Ras + AKT murine models and found that it reduced the incidence of HCC by inhibiting the Cyclin D-CDK4/6-INK4-Rb pathway and inducing senescence in hTICs. In addition, we observed the activation of the Cyclin D-CDK4/6-INK4-Rb pathway in the progression from CLI to HCC, according to the human precancerous stage samples, indicating the clinical translation prospects of PD-0332991 for pre-HCC intervention. In summary, under the premise of limited HCC intervention measures, we explored a new strategy for early intervention prior to HCC formation by inducing hTICs senescence.

Results

PD-0332991 effectively inhibited hepatocarcinogenesis in CLI mouse models

In our previous study about inducing CLI by low-dose NTBC (2.5 % blocking dose, 187.5 μg/L), we observed 100 % incidence of HCC in $Fah^{-/-}$ mice after 12 weeks of CLI [21]. To study the effect of the CDK4/6 inhibitor, PD-0332991, on CLI-induced hepatocarcinogenesis, PD-0332991 was administered to $Fah^{-/-}$ mice with 8-week CLI for four weeks (Figure S1A). Interestingly, the incidence of HCC decreased from 100 % to 29.15 % (Fig. 1A and 1B) compared with that in the control group. Both the sizes and numbers of tumors were significantly reduced (Fig. 1B). At 8-week CLI mouse liver tissues, some hepatocytes showed large cell changes [26] with enlarged nuclei characterized by nuclear heterogeneity. This

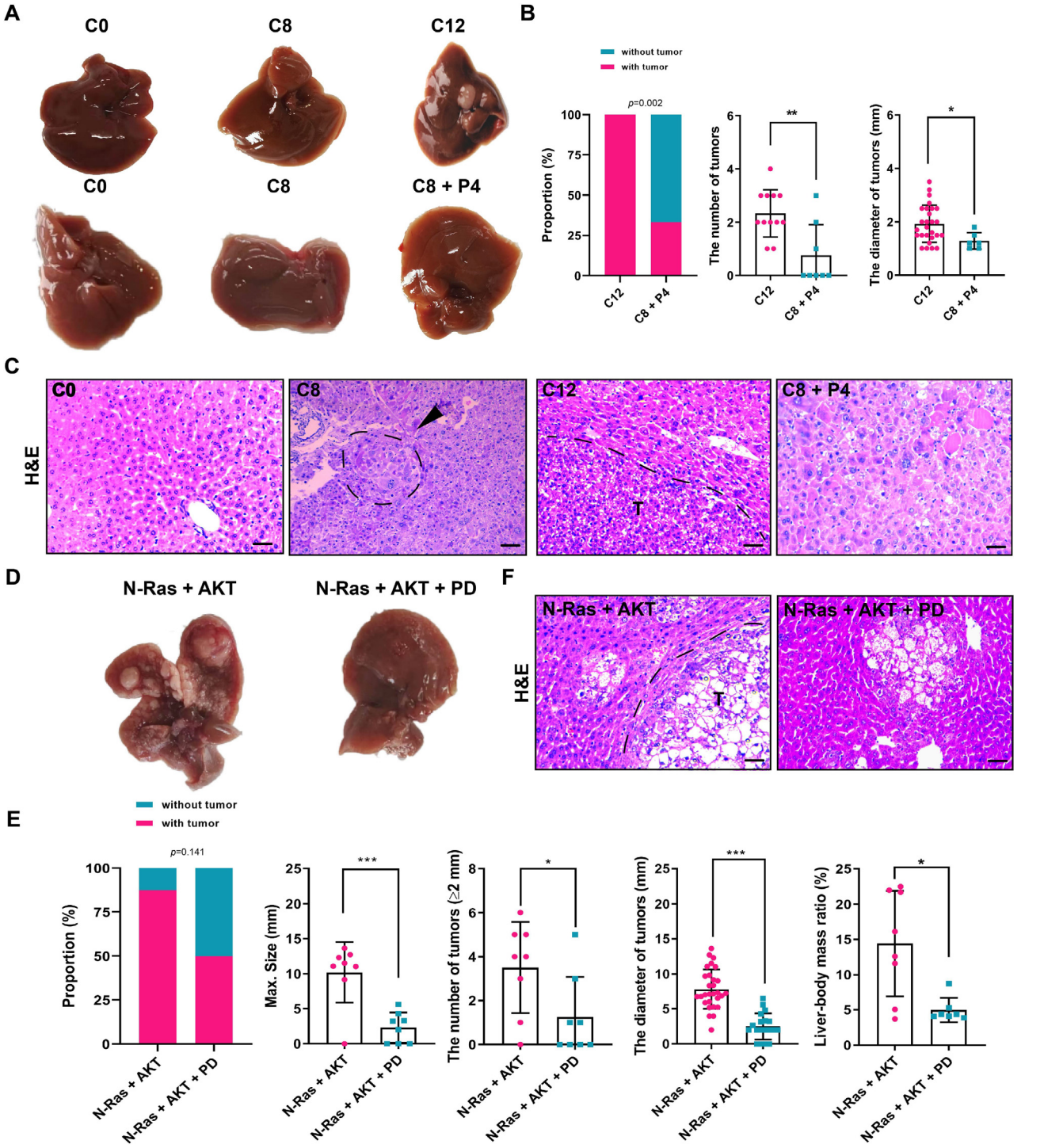

Fig. 1. PD-0332991 prevents hepatocarcinogenesis in mice with chronic liver injury. (A) Liver appearance of *Fah*$^{-/-}$ mice before and after administration of PD-0332991. C0 group represents *Fah*$^{-/-}$ mice induced with CLI for 0 weeks, C8 group represents *Fah*$^{-/-}$ mice induced with CLI for 8 weeks, C12 group represents *Fah*$^{-/-}$ mice induced with CLI for 12 weeks, C8 + P4 group represents *Fah*$^{-/-}$ mice induced with CLI for 12 weeks and received additional PD-0332991 gavage for the latter 4 weeks. (B) Graphs representing the HCC incidence of *Fah*$^{-/-}$ mice with or without PD-0332991 gavages (C12 and C8 + P4 group), scatter plots displaying the tumor numbers (C12 group: 2.33 ± 0.89 and C8 + P4 group: 0.75 ± 1.17. Values are shown in mean ± SD) and size of tumors (C12 group: 1.92 ± 0.70 mm and C8 + P4 group: 1.28 ± 0.31 mm. Values are shown in mean ± SD); n = 10–12 mice/group. (C) H&E staining of the livers in the C0, C8, C12, and C8 + P4 group mice. The dash circle pointed by arrowheads in the graphs of the C8 group represents focal heterogeneous hyperplasia; the letter T in the graphs of the C12 group represents the HCC nodules, and the dash line shows the boundaries of the HCC nodules. (D) Comparison of liver appearance and tumorigenesis in C57 BL/6J mice after N-Ras + AKT proto-oncogene plasmids injection, with or without PD-0332991 gavages; N-Ras + AKT group represents C57 BL/6J mice 6 weeks after plasmids injection; N-Ras + AKT + PD group represents C57 BL/6J mice 6 weeks after plasmids injection and treated with PD-0332991 for the latter 4 weeks. (E) HCC incidence, maximum tumor diameter (N-Ras + AKT group: 10.18 ± 4.32 mm and N-Ras + AKT + PD group: 2.23 ± 2.15 mm. Values are shown in mean ± SD), number of tumors (N-Ras + AKT group: 3.5 ± 2.07 and N-Ras + AKT + PD group: 1.25 ± 1.832. Values are shown in mean ± SD), tumor size (N-Ras + AKT group: 7.82 ± 2.81 mm and N-Ras + AKT + PD group: 2.50 ± 1.86 mm. Values are shown in mean ± SD), and liver-body weight ratio statistics for the N-Ras + AKT group and the N-Ras + AKT + PD group; n = 8 mice/group. (F) H&E staining of the livers from mice of N-Ras + AKT group and N-Ras + AKT + PD group. (Scale bar is 50 μm; *, $p < 0.05$; **, $p < 0.01$; ***, $p < 0.001$).

change was more prominent in well-bordered HCC nodules at 12 weeks of CLI. However, the development of HCC was significantly delayed after PD-0332991 treatment (Fig. 1C), and mice with CLI that were treated with PD-0332991 showed alleviated liver injury (Figure S1B).

To validate the results obtained in the CLI-HCC *Fah*$^{-/-}$ mouse model, another canonical CLI-HCC mouse model was used. Specifically, simultaneous injection of N-Ras and AKT oncogene overexpressing plasmids caused nodular and diffuse HCC formation in mice, mimicking the progression from nonalcoholic fatty liver disease (NAFLD) to HCC in mice [27]. Ninety percent of the N-Ras + AKT mice developed CLI after injection of the N-Ras + AKT plasmid, followed by spontaneous hepatocarcinogenesis six weeks after injection. Two weeks after injection of the N-Ras + AKT plasmid, PD-0332991 was administered to N-Ras + AKT mice for four weeks (Figure S1C). In line with the results in CLI-HCC *Fah*$^{-/-}$ mice, two weeks after plasmids injection, the HCC incidence of N-Ras + AKT mice following PD-0332991 treatment for four weeks dropped to 50 % (Fig. 1D and 1E). Moreover, the number of tumors, tumor diameter, maximal tumor diameter, and liver weight ratio (liver weight: body weight) were notably reduced in the PD-0332991 treatment group (Fig. 1E). Hematoxylin-eosin (HE) staining showed that the number of tumor nodules also noticeably decreased in N-Ras + AKT mice treated with PD-0332991 (Fig. 1F). Additionally, the degree of liver injury in N-Ras + AKT mice was alleviated after administration of PD-0332991 (Figure S1D). Collectively, these results revealed that the cell cycle inhibitor PD-0332991 effectively prevented hepatocarcinogenesis in CLI.

PD-0332991 induced hepatocellular senescence but not apoptosis in mice with CLI

To investigate the reasons for the reduced incidence of HCC in two CLI mouse models, we firstly studied whether PD-0332991 affected cellular senescence in pre-HCC stages via detecting the expression changes of cellular senescence markers, including SA-β-Gal and P21 and also SASP factors [28,29]. Consequently, we discovered that the liver tissues of *Fah*$^{-/-}$ mice with PD-0332991 treatment had more SA-β-Gal positive cells than those of *Fah*$^{-/-}$ mice with CLI after 0, 8, and 12 weeks (Fig. 2A and 2B). Accordingly, we detected more P21^{+} hepatocytes in *Fah*$^{-/-}$ mice with PD-0332991 treatment than in other groups (Fig. 2A and 2B). Furthermore, co-staining of P21 and SA-β-Gal demonstrated that SA-β-Gal^{+} cells were co-localized with P21^{+} cells (Figure S1E). In addition, we also found a considerably higher proportion of SA-β-Gal^{+} and P21^{+} cells in the livers of the N-Ras + AKT + PD group than in the untreated group (Fig. 2C and 2D). Similarly, co-staining confirmed that the distribution of SA-β-Gal^{+} cells was indeed consistent with P21^{+} cells in the livers of the mice from N-Ras + AKT group and N-Ras + AKT + PD group (Figure S2A).

We then analyzed the changes in the expression of SASP factors in liver samples from the C12 and C8 + P4 groups of *Fah*$^{-/-}$ mice. The quantitative analyses showed that the expression levels of key inflammatory factors (CCL2, CCL4, CCL20, and CXCL10) were elevated in the liver samples from *Fah*$^{-/-}$ mice treated with PD-0332991. Moreover, the decreased expression of Lamin B1, a nuclear intermediate filament protein and marker of senescent cells (Fig. 2E), further suggested that PD-0332991 induced cellular senescence in some hepatocytes of *Fah*$^{-/-}$ mice.

Some studies have revealed that PD-0332991 induces apoptosis in a variety of tumor cells, and in particular cell types, apoptosis and cellular senescence pathways exhibit antagonism towards each other [30,31]. To determine whether PD-0332991 induced hepatocyte apoptosis, TUNEL staining of liver tissues from all groups of *Fah*$^{-/-}$ mice and N-Ras + AKT mice was performed. No apoptotic hepatocytes were stained in the liver tissues of either mouse model under the different treatment protocols (Fig. 2A-D).

PD-0332991 induced senescence of TICs in the liver of mice with CLI

As somatic hepatocytes lose their ability to proliferate and renew under CLI [32,33], we speculated that PD-0332991 mainly targets proliferating hepatocytes and cells that has partially or fully undergone malignant transformation, and induces cellular senescence in these. MCM2 is a component of the DNA replication initiation complex that is assembled only in the nucleus of proliferating cells and is stably present throughout the cell cycle, including the G1, S, G2, and M phases [34,35]. Therefore, we selected MCM2 to identify proliferating and quiescent (G0 phase) hepatocytes.

Subsequently, immunofluorescence co-staining revealed that the proportion of MCM2^{+} cells was significantly reduced in mice treated with PD-0332991 compared to that in the control group. Interestingly, a predominant subset of cells expressing MCM2 concurrently demonstrated positive immunostaining for P21 (Fig. 3A and S2B). This result demonstrated that PD-0332991 selectively induced the senescence of proliferating (non-G0 phase) hepatocytes in the liver, whereas it did not induce cellular senescence in hepatocytes in the quiescent state (G0 phase).

In advanced CLI, hTICs is a subset of hepatocytes that exhibits aberrant proliferation. We further identified whether the induced senescent cells were mainly derived from these malignant-transformed hepatocytes in the precancerous stage using a series of hTIC-associated stemness markers, including PCNA, AFP, Ki-67, EpCAM, GST-Pi, and CK19 [36,37], and found that hTICs appeared in the livers of *Fah*$^{-/-}$ mice at eight weeks of CLI, as well as in N-Ras + AKT mice at six weeks of CLI (Fig. 3B and S2C). The hTICs gradually accumulated in the liver during CLI without intervention. However, PD-0332991 reduced the number of hTICs in the liver, which positively correlated with a decline in the incidence of HCC (Fig. 3C and S2D). Glutathione-S-transferase (GSTp) is highly expressed in TICs from multiple precancerous tissues and is associated with poor patient prognosis [38,39]. Using immunofluorescence co-staining of P21 and GSTp, we found that the senescent cells were co-localized with that of hTICs in the liver sections of PD-0332991 treated mice, suggesting that after administration of PD-0332991 senescence was induced in livers of mice with CLI (Fig. 3D and S2E).

PD-0332991 induced senescence of hTICs isolated from chronically injured livers in vitro

To further elaborate the role of PD-0332991 in targeting hTICs to induce cellular senescence, hTICs were isolated from the livers of *Fah*$^{-/-}$ mice with 8-weeks CLI and N-Ras + AKT plasmid injected mice (four weeks after injection). After harvesting the cells by *in situ* collagenase perfusion, non-aggregated hepatocytes were dispersed into single cells, whereas precancerous cells remained clustered owing to collagenase resistance (Fig. 4A and S3A) [36,37]. The expression of human HCC markers, such as CD44, EpCAM, GPC3, CLDN2 and AFP, was upregulated in clustered aggregated hepatocytes (TICs) compared to that in non-aggregated hepatocytes (non-TICs), but at lower levels than in HCC cells [36] (Fig. 4B and S3B). Furthermore, hTICs expressed AFP, SOX9, CK19, CD44, EpCAM, GSTp and ALB, whereas non-TICs expressed only ALB (Fig. 4C and S3C). Altogether, these results revealed that the aggregated cells isolated from the chronically injured livers of the two murine models were mainly hTICs, and the tumorigenicity of hTICs were intermediate between that of normal hepatocytes and HCC cells.

After *in vitro* sorting and characterization of hTICs from mice, we verified the invasiveness of the isolated hTICs. We transplanted

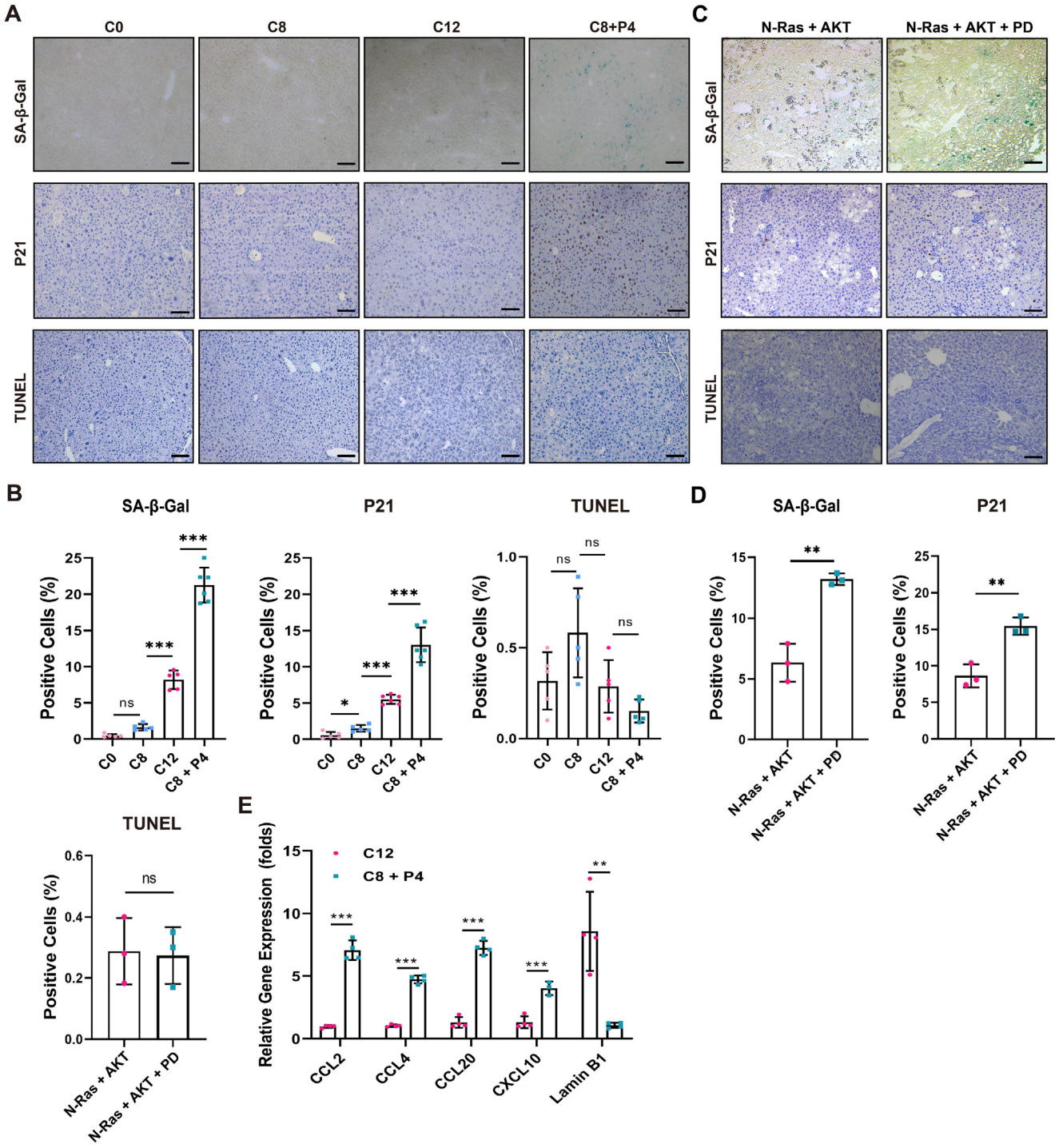

Fig. 2. PD-0332991 induced liver senescence in *Fah*$^{-/-}$ mice and N-Ras + AKT mice. (A) IHC staining of SA-β-Gal, P21 and TUNEL in liver tissues of *Fah*$^{-/-}$ mice from C0, C8, C12, C8 + P4 group. (B) Statistical analysis of the proportion of SA-β-Gal^{+} cells, P21^{+} cells and apoptotic cells in liver tissue of *Fah*$^{-/-}$ mice before and after PD-0332991 administration. (C) IHC staining of SA-β-Gal, P21 and TUNEL in liver tissues from the N-Ras + AKT group and the N-Ras + AKT + PD group. (D) Statistical analysis of the proportion of SA-β-Gal^{+} cells, P21^{+} cells and apoptotic cells in liver tissue from the N-Ras + AKT group and the N-Ras + AKT + PD group. (E) RT-qPCR analysis of SASP factor genes (CCL2, CCL4, CCL20, CXCL10, and Lamin B1) expression in liver samples of *Fah*$^{-/-}$ mice with or without PD-0332991 administration. (Relative gene expression of CCL2 in C12 group: 0.96 ± 0.11 and C8 + P4 group: 7.06 ± 0.78; relative gene expression of CCL4 in C12 group: 1.04 ± 0.10 and C8 + P4 group: 4.73 ± 0.32; relative gene expression of CCL20 in C12 group: 1.30 ± 0.43 and C8 + P4 group: 7.26 ± 0.56; relative gene expression of CXCL10 in C12 group: 1.32 ± 0.48 and C8 + P4 group: 4.03 ± 0.53; relative gene expression of Lamin B1 in C12 group: 8.57 ± 3.16 and C8 + P4 group: 1.07 ± 0.22. All values are folds and shown in mean ± SD). (Scale bar is 50 μm; n = 3–6 mice/group; *, $p < 0.05$; **, $p < 0.01$; ***, $p < 0.001$).

hTICs (1×10^6) into the livers of *Fah*$^{-/-}$ mice with four weeks of CLI *in situ*. As expected, the number of secondary HCC nodes were higher in the hTICs transplanted group than that in the control group (non-TICs transplanted *Fah*$^{-/-}$ mice) (Fig. 4D).

To verify the sensitivity of PD-0332991, clustered hTICs and non-TICs from the two CLI murine models were cultured *in vitro* and subjected to PD-0332991 treatment. The half maximal inhibitory concentration (IC_{50}) value of hTICs (IC_{50} = 2.562), derived from

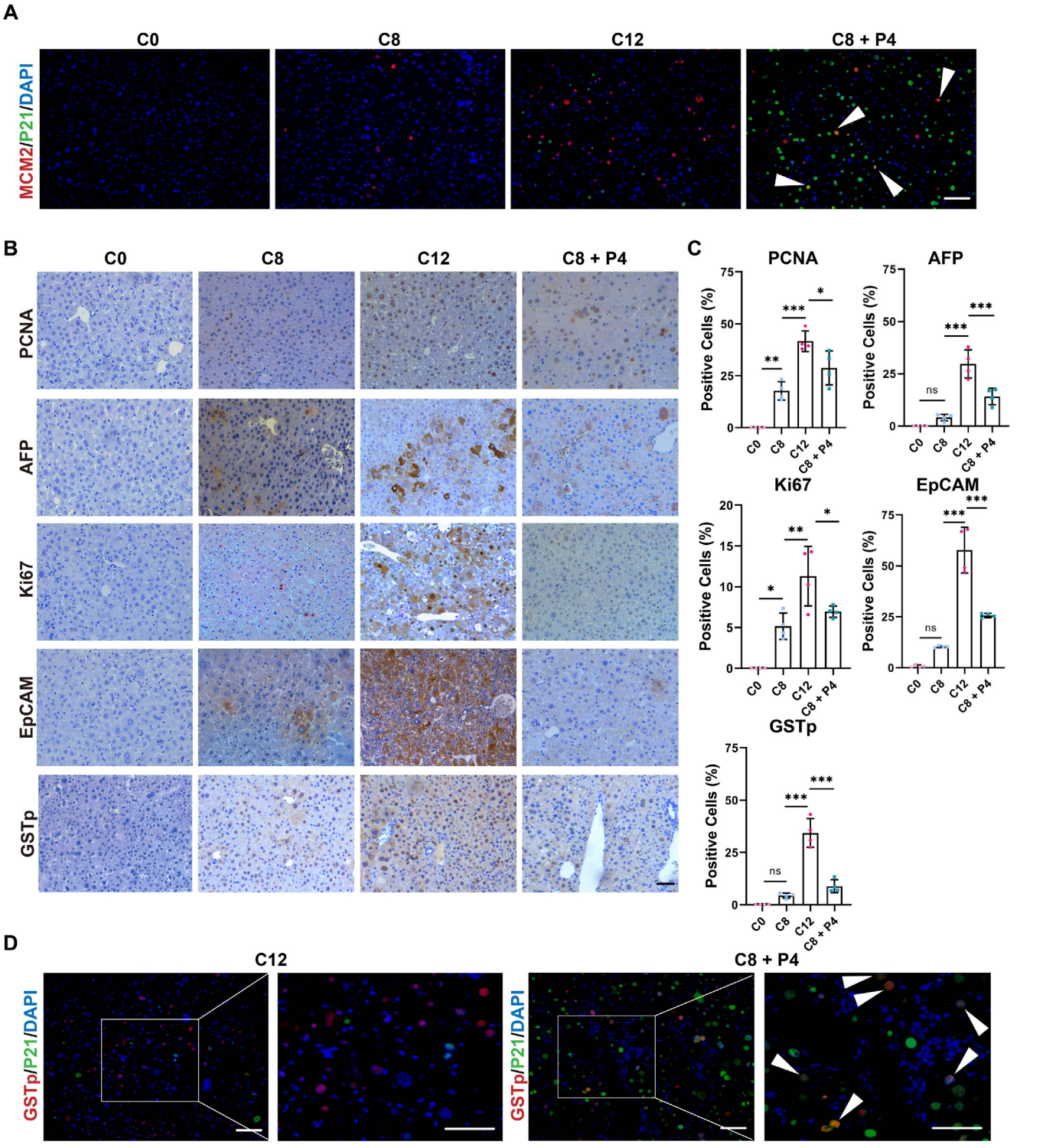

Fig. 3. PD-0332991 induced senescence of hTICs in *Fah*$^{-/-}$ mice with chronic liver injury. (A) Immunofluorescence co-staining of proliferation marker (MCM2) and senescence marker (P21) in liver samples from mice of the C0, C8, C12, and C8 + P4 group, the arrows showing MCM2$^+$/P21$^+$ hepatocytes. The proportion of MCM2$^+$/P21$^+$ cells among MCM2$^+$ cells in C12 group was 0.64 % ± 0.07 %. The proportion of MCM2$^+$/P21$^+$ cells among MCM2$^+$ cells in C8 + P4 group was 35.4 % ± 2.97 %. (B-C) IHC staining of TICs indicators (PCNA, AFP, Ki67, EpCAM, and GSTp) in liver tissues from *Fah*$^{-/-}$ mice of the C0, C8, C12, and C8 + P4 group, and quantitative analysis of PCNA$^+$, AFP$^+$, Ki67$^+$, EpCAM$^+$, and GSTp$^+$ cells. (D) Immunofluorescence co-staining of P21 and GSTp in serial sections of liver tissues of *Fah*$^{-/-}$ mice in C12 and C8 + P4 group. The proportion of GSTp$^+$/P21$^+$ cells among GSTp$^+$ cells in C12 group was 0.40 % ± 0.23 %. The proportion of GSTp$^+$/P21$^+$ cells among GSTp$^+$ cells in C8 + P4 group was 38.87 % ± 9.64 %. (Scale bar is 50 μm; n = 4 for both group; *, $p < 0.05$; **, $p < 0.01$; ***, $p < 0.001$).

the *Fah*$^{-/-}$ mice with 8-weeks CLI, was lower than the non-TICs (IC_{50} = 4.859), and similar to those derived from the N-Ras + AKT mice (2.0 *versus* 3.679), indicating that hTICs were more sensitive to PD-0332991 than non-TICs (Fig. 4E and S3D). Consistently, the proliferation rate of hTICs was significantly higher than that of non-TICs without intervention, whereas after PD-0332991 treatment (2 μM), the proliferation capacity of hTICs decreased more severely than that of non-TICs (Fig. 4F, G and S3E). Moreover, the

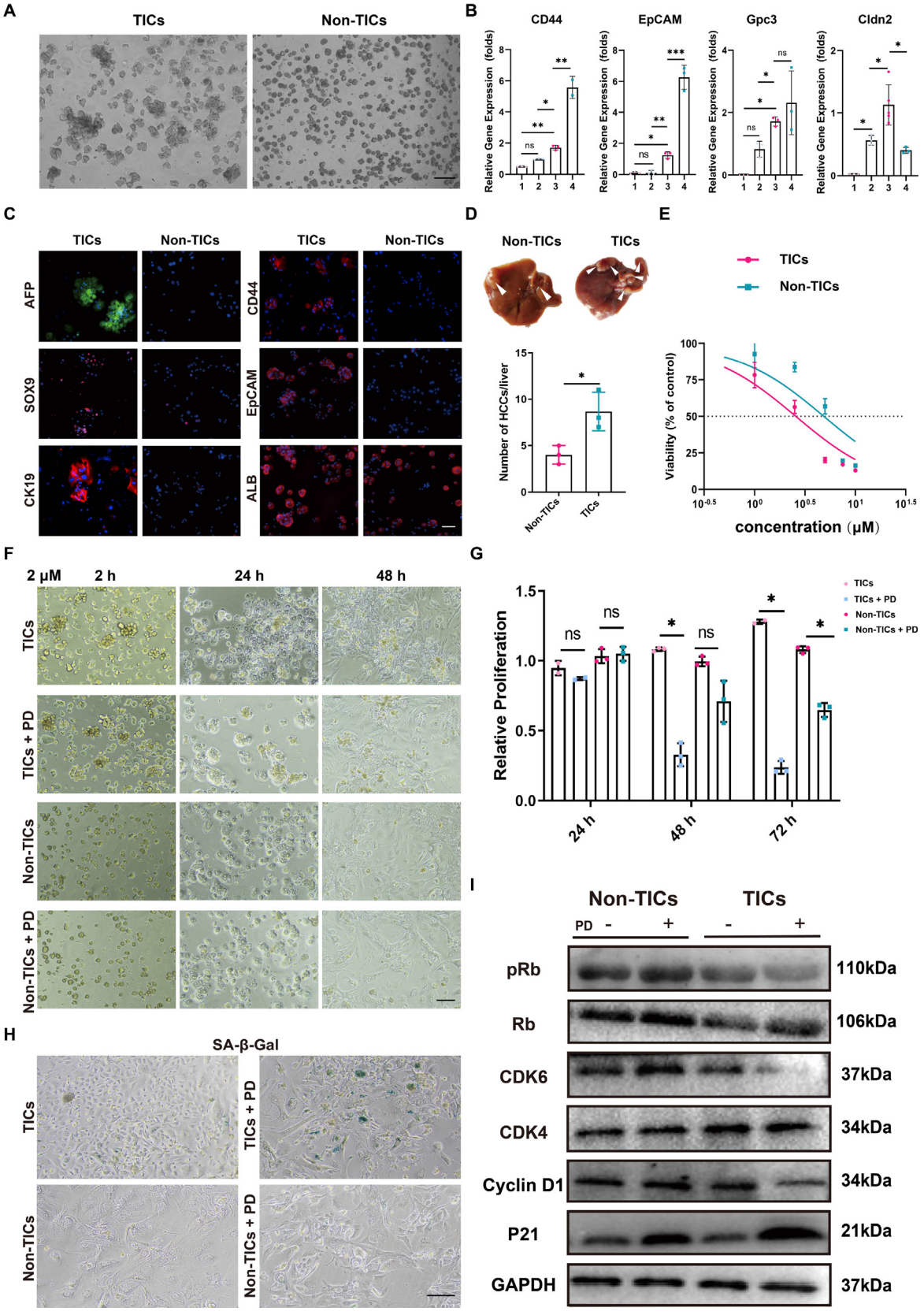
A
TICs
Non-TICs
B
CD44
EpCAM
Gpc3
Cldn2
Relative Gene Expression (folds)
C
TICs
Non-TICs
AFP
SOX9
CK19
CD44
EpCAM
ALB
D
Non-TICs
TICs
Number of HCCs/liver
E
TICs
Non-TICs
Viability (% of control)
concentration (μM)
F
2 μM
2 h
24 h
48 h
TICs
TICs + PD
Non-TICs
Non-TICs + PD
G
TICs
TICs + PD
Non-TICs
Non-TICs + PD
Relative Proliferation
24 h
48 h
72 h
H
SA-β-Gal
TICs
TICs + PD
Non-TICs
Non-TICs + PD
I
Non-TICs
TICs
PD
pRb
Rb
CDK6
CDK4
Cyclin D1
P21
GAPDH
110kDa
106kDa
37kDa
34kDa
34kDa
21kDa
37kDa

proportion of SA-β-Gal$^+$ hTICs was increased after 48 h of PD-0332991 treatment (Fig. 4H and S3F), which further revealed that PD-0332991 could specifically induced senescence of hTICs.

To further analyze the underlying mechanism by which PD-0332991 induces cellular senescence in hTICs *in vitro*, we analyzed the protein expression of the relevant signaling pathways. The levels of phosphorylated Rb (pRb) and Cyclin D1 in hTICs were significantly decreased following PD-0332991 treatment for 48 h (Fig. 4I and S3G-I), whereas the level of P21 increased. These results indicated that PD-0332991 induced senescence in hTICs by effectively inhibiting the activation of the Cyclin D-CDK4/6-INK4-Rb pathway and repressing the phosphorylation of Rb protein, which in turn inhibited the G1/S transition of hTICs and ultimately led to senescence, thus inhibiting HCC occurrence.

PD-0332991 inhibited the activation of the Cyclin D-CDK4/6-INK4-Rb pathway during progression from CLI to HCC

In various tumors, including HCC, over-activation of the Cyclin D-CDK4/6-INK4-Rb pathway is closely related to occurrence, progression, and poor prognosis of disease [15,40,41]. However, in precancerous lesions, the understanding of this pathway remains ambiguous.

In human CLI, HCC generally develops after low-degree fibrosis (FL), high-degree fibrosis (FH), cirrhosis (CS), and dysplastic nodules (DN). This chronological phase also reflects the precancerous histopathological grades [42,43]. To explore the pathway changes during the transition from precancerous lesions to HCC, we obtained RNA-seq data from 15 normal samples, 47 human CLI samples, and 54 HCC samples from GSE148355 in the Gene Expression Omnibus (GEO) database (Fig. 5A). In the dataset, DN were further categorized as low-grade DN (DL) or high-grade DN (DH), based on the degree of differentiation [44]. The histopathological grades of the HCC samples were divided into TG1, TG2, and TG3 stages (TG1/2/3, estimated by the Edmonson and Steiner classification). Gene ontology (GO) enrichment analysis was performed on the upregulated genes in all samples. The results showed that immune-related signals were activated in the period preceding DL development, especially in B cell-related immune response pathways (Figure S4A). Later, a series of cell cycle-related pathways were gradually enriched in the DL, DH, and TG1 samples, indicating that the cell cycle was already activated in precancerous lesions (Fig. 5B, 5C, S4A).

Next, we evaluated the activation score of the Cyclin D-CDK4/6-INK4-Rb pathway in these datasets using single-sample gene set enrichment analysis (ssGSEA) and found that the pathway activation scores were highlighted in precancerous lesions and reached the highest level in DL samples (Fig. 5D). Notably, in precancerous FH, CS, and DL samples, the signature scores of the Cyclin D-CDK4/6-INK4-Rb pathway were higher than those of the HCC-initiated TG1, TG2, and TG3 samples. In contrast, the activation scores of other cell cycle-related pathways, including E2F targets, mitotic spindles, and G2/M checkpoints, were highest in TG2 and TG3 (Figure S4B). This suggests that for most *RB1* mutation-free patients, targeted intervention of the Cyclin D-CDK4/6-INK4-Rb pathway in precancerous lesions may be more appropriate than in HCC to prevent TICs from progressing to HCC.

To verify whether a similar trend also occurred before and after treatment with PD-0332991 on hepatocytes and hTICs, transcriptome sequencing analysis was performed on the liver tissues of *Fah*$^{-/-}$ mice with CLI and *Fah*$^{-/-}$ mice treated with PD-0332991. Using the R software package Mfuzz (version: 2.54.0) [45] to perform gene clustering and screen out gene clusters with the same continuous trends in the sequenced data, we observed that the two clusters showed significant changes, and the expression levels of genes in Cluster 4 increased with the progression of CLI and decreased after PD-0332991 treatment. However, the trend in gene expression changes in cluster 6 was opposite to that in cluster 4 (Fig. 5E and S4C). We further studied the functions of genes in clusters 4 and 6 through GO analysis, and the results indicated that genes in cluster 4 were mainly enriched in the cell cycle, RNA splicing *etc.* Genes in cluster 6 were mainly enriched in fatty acid and lipid metabolisms *etc.* (Fig. 5E), suggesting that cell cycle-related pathways were gradually activated, whereas metabolism-related pathways were gradually inhibited during the progression of CLI, indicating that PD-0332991 treatment suppressed cell cycle-related pathways and activated metabolism-related pathways. Correspondingly, decreased Oil Red Staining were observed in the livers of CLI mice with PD-0332991 treatment, compared with controls (Figure S5A and S5B). Similarly, the gene set score of the Cyclin D-CDK4/6-INK4-Rb pathway, composed of *CDK4*, *CDK6*, *CDK2*, *RB1*, *CCND1*(Cyclin D1), *CDKN2A* (p16), and *CDKN1A* (p21), was consistent with that of cluster 4 (Fig. 5F).

We then verified whether these trends were also present in protein-level changes. We extracted proteins from liver samples of *Fah*$^{-/-}$ mice with different degrees of CLI and detected the expression levels of Cyclin D-CDK4/6-INK4-Rb pathway-related proteins. The protein expression levels of Cyclin D1, CDK4, CDK6, pRb, and other key proteins increased with CLI progression (Fig. 6A-B). RNA-seq analysis showed that cell cycle-related genes were significantly downregulated in *Fah*$^{-/-}$ mice following PD-0332991 treatment, especially Cyclin D1 (Fig. 6C). We also found that the levels of pRb and Cyclin D1 noticeably decreased (Fig. 6D-E), indicating that PD-0332991 inhibited cell proliferation by targeting the

Fig. 4. *In vitro* characterization of TICs isolated from chronically injured livers of *Fah*$^{-/-}$ mice and their senescence induced by PD-0332991. (A) Hepatic TICs and non-TICs were obtained from the livers of *Fah*$^{-/-}$ mice in C8 group after perfusion. TICs are aggregated in small clusters due to collagenase resistance (left), and non-aggregated hepatocytes (non-TICs) without collagenase resistance are dispersed as individual cells (right). (B) RT-qPCR analysis of HCC markers (CD44, EpCAM, Gpc3 and Cldn2) was conducted in hTICs, non-TICs from the livers of *Fah*$^{-/-}$ mice in C8 group and HCC cells isolated from the livers of *Fah*$^{-/-}$ mice in C12 group, and compared with those in perfusion-isolated hepatocytes from *Fah*$^{-/-}$ mice in C0 group (without CLI); 1. Hepatocytes from the livers of *Fah*$^{-/-}$ mice in C0 group; 2. non-aggregated hepatocytes (non-TICs) from *Fah*$^{-/-}$ mice in C8 group; 3. Aggregated hTICs from *Fah*$^{-/-}$ mice in C8 group; 4. HCC cells from *Fah*$^{-/-}$ mice in C12 group. (Relative gene expression of CD44 in 1, 2, 3 and 4, respectively: 0.51 ± 0.03, 0.96 ± 0.05, 1.71 ± 0.15 and 5.57 ± 0.71; relative gene expression of EpCAM in 1, 2, 3 and 4, respectively: 0.11 ± 0.07, 0.10 ± 0.16, 1.25 ± 0.21 and 6.26 ± 0.77; relative gene expression of Gpc3 in 1, 2, 3 and 4, respectively: 0.02 ± 0.01, 0.83 ± 0.25 folds, 1.71 ± 0.15 and 2.31 ± 1.03; relative gene expression of Cldn2 in 1, 2, 3 and 4, respectively: 0.04 ± 0.02, 0.56 ± 0.08, 1.13 ± 0.32 and 0.40 ± 0.05. All values are folds, values are shown in mean ± SD). (C) Hepatic TICs and non-TICs obtained from the livers of *Fah*$^{-/-}$ mice in C8 group were stained with the TICs markers including AFP, SOX9, CK19, CD44, EpCAM and ALB. (D) Statistics for the number of HCC nodules in the livers of CLI *Fah*$^{-/-}$ mice four weeks after the *in situ* injection of isolated non-TICs and TICs; n = 3 mice/group. (E) Isolated hTICs and non-TICs were obtained from the livers of the same *Fah*$^{-/-}$ mice described in (C), and treated with PD-0332991 for IC_{50} assay. (F) Effect of PD-0332991 (2 μM) on proliferation of isolated hTICs and non-TICs within 48 h, PD-0332991 is abbreviated as PD. (G) CCK8 assay of isolated hTICs and non-TICs, incubated with or without PD-0332991 (2 μM) for 24 h, 48 h, 72 h. (H) SA-β-Gal staining of isolated hTICs and non-TICs, following the culture experiments shown in (F). (I) Immunoblotting of Cyclin D-CDK4/6-INK4-Rb signaling-related proteins (CDK4, CDK6, Cyclin D1, pRb and other proteins) expression in hTICs and non-TICs isolated from the livers of *Fah*$^{-/-}$ mice in C8 group, incubated with or without PD-0332991. (Scale bar is 50 μm; n = 3 for both group; *, $p < 0.05$; **, $p < 0.01$; ***, $p < 0.001$).

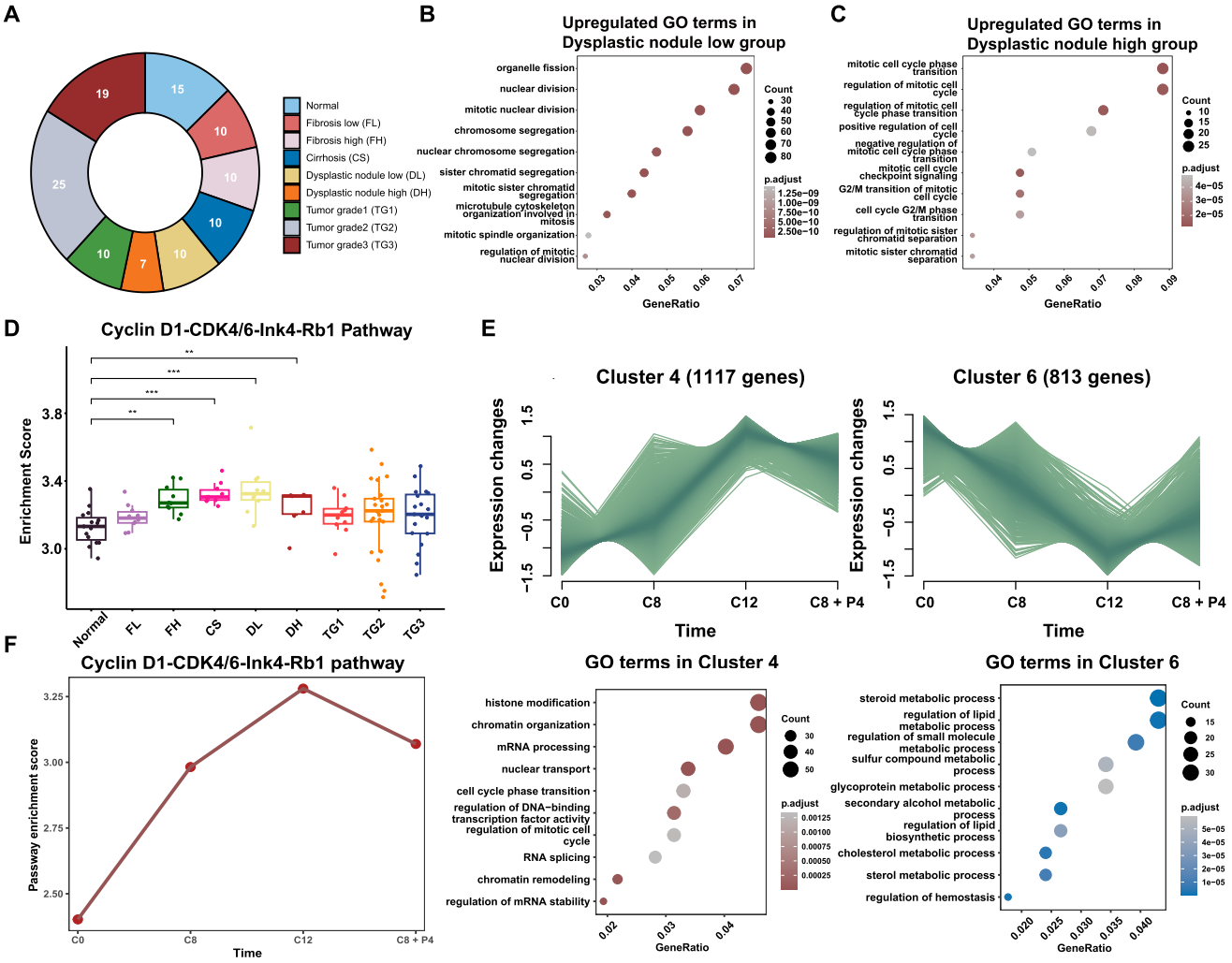

Fig. 5. Expression analysis of the Cyclin D-CDK4/6-INK4-Rb pathway during the progression from chronic liver injury to HCC. (A) Composition and proportion of cases with different pathological histological features in the data source; Normal (non-tumor normal control), FL (Fibrosis low), FH (Fibrosis high), CS (Cirrhosis), DL (Dysplastic nodule low), DH (Dysplastic nodule high), TG1 ~ 3 (TG1, TG2 and TG3 estimated by the Edmonson and Steiner classification). (B) Comparing results of up-regulated gene sets between samples from DL group and Normal group, gene sets analyzed by GO enrichment analysis. (C) Comparing results of up-regulated gene sets between samples from DH group and Normal group, gene sets analyzed by GO enrichment analysis. (D) Diagram of the expression of the Cyclin D-CDK4/6-INK4-Rb pathway in the clinical liver samples with different degrees of CLI, pathway scores were obtained by ssGSEA algorithm calculation. (E) The gene profiles were classified into 9 Clusters with consistent expression trends using Mfuzz analysis, Cluster 4 is on the upper left and Cluster6 is on the upper right, other clusters are shown in Supplementary Fig. 4C; The top 10 GO terms of genes in Cluster 4 (lower left) and Cluster 6 (lower right) were determined by GO enrichment analysis using the ClusterProfiler R-package. (F) Changes in expression levels of genes in the Cyclin D-CDK4/6-INK4-Rb signaling pathway set in the C0, C8, C12, and C8 + P4 group, and the overall expression levels of the gene set were assessed using the ssGSEA algorithm.

Cyclin D-CDK4/6-INK4-Rb pathway. The same pattern was detected in the N-Ras + AKT mice (Figure S6A). PD-0332991 also reduced the phosphorylation level of CDK6 in the liver of both CLI mouse models, indicating its role as an effective CDK4/6 inhibitor (Fig. 6D-E and S6A).

At the transcriptome level, we observed consistent changes in cell cycle-related pathways, particularly the Cyclin D-CDK4/6-INK4-Rb pathway, in human samples and in the two murine models. Aberrant activation of the cell cycle has been observed in both DN and hTICs, which are precancerous lesions. This pathway was effectively inhibited by PD-0332991. The therapeutic strategy of targeting the Cyclin D-CDK4/6-INK4-Rb pathway using PD-0332991 in the CLI stage exhibited promising clinical translational potential for reducing the incidence of HCC.

Senescence surveillance of hTICs suppresses hepatocarcinogenesis

SASP factors can trigger senescence in an autocrine or paracrine fashion and thereby enhance the anti-tumor effect [46,47]. Eggert *et al.* demonstrated that the secretion of CCL2 from senescent pre-malignant hepatocytes orchestrates the recruitment of $CCR2^{+}$ immature myeloid cells (iMC). These iMC differentiate into macrophages that clear the pre-malignant senescent cells [48].

Quantitative polymerase chain reactions (PCR) and immunoblotting validation confirmed the increased expression of pivotal SASP factors. Analysis and verification revealed elevated expressions of two SASP factors, CCL2 and CXCL10, in the livers of PD-0332991-treated CLI mice, as well as in senescent hTICs *in vitro* (Fig. 7A-C and S6B-D). CCL2 and CXCL10 play central roles

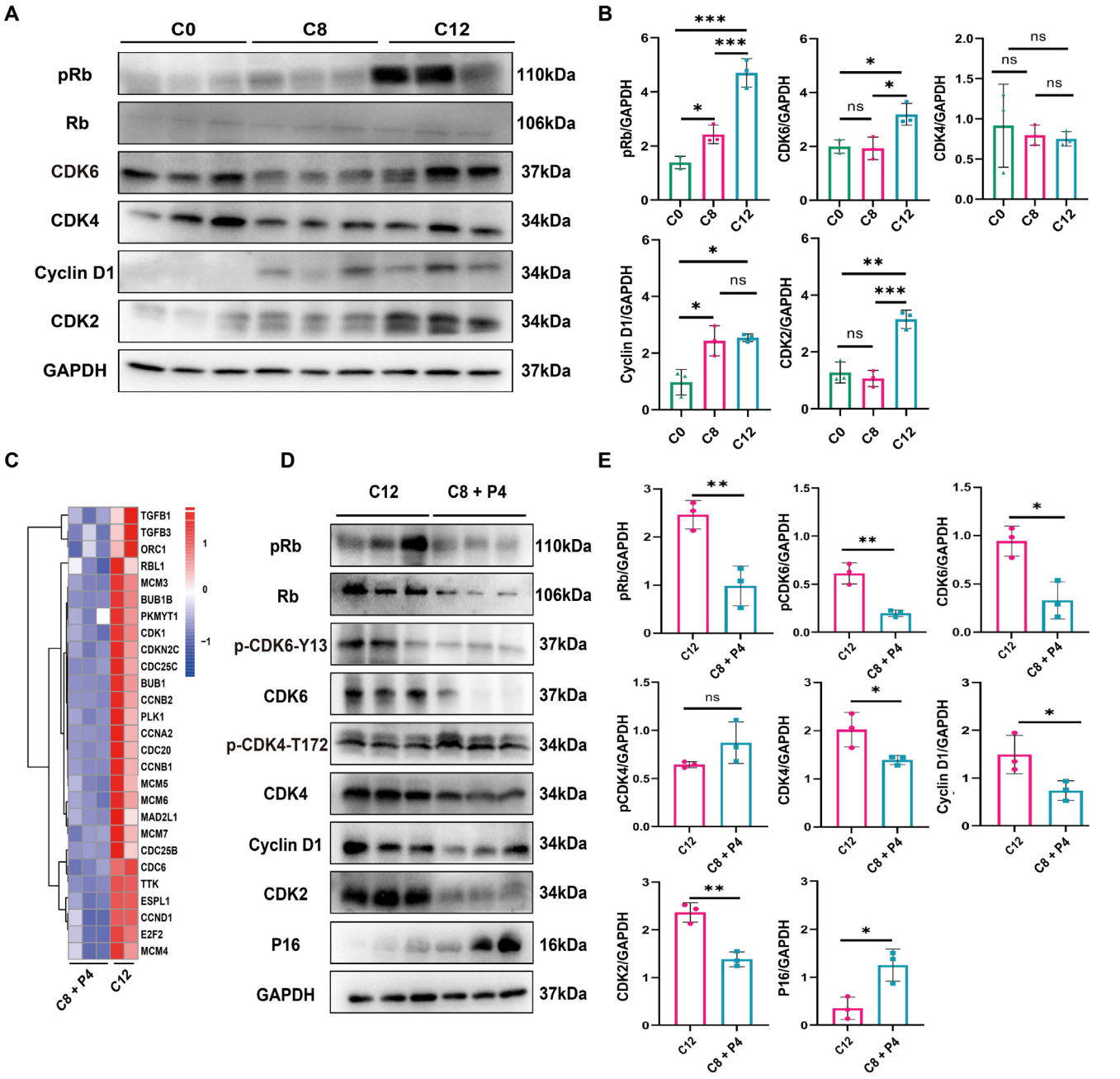

Fig. 6. Upregulation of the Cyclin D-CDK4/6-INK4-Rb pathway during hepatocarcinogenesis in chronic liver injury. (A-B) Immunoblot validation of Rb, pRb, CDK4/6, Cyclin D1 and CDK2 in liver tissues from mice in C0 group, C8 group and C12 group, and the relative expression analysis of these proteins. (C) Heatmap of relative transcription level of key regulating genes of the Cell Cycle term, compared between the samples from the C12 and C8 + P4 group. (D-E) Immunoblot validation of the expression of Cyclin D1, pRb, CDK4, CDK6 and other proteins in C12 group and C8 + P4 group, and statistical analysis of differences in expression. (n = 3 for both group; *, $p < 0.05$; **, $p < 0.01$; ***, $p < 0.001$).

in directing monocyte and macrophage chemotaxis and in facilitating the recruitment of effector cells to inflammatory sites. This orchestrated response enhances immune surveillance and exerts substantial effects on the early stages of tumorigenesis [49]. Quantitative PCR further identified augmented expression of F4/80 and CD86 in the livers of CLI mice treated with PD-0332991, which suggested an increase in M1 macrophage infiltration into the liver tissue of CLI mice (Fig. 7D and S6E). Macrophages express a range of CXCL and CCL family receptors, particularly CCR2 and CXCR3, on their surfaces. CCL2 and CXCL10 effectively bind to these receptors and activate adaptive immune responses [50,51]. In PD-0332991-treated CLI mice, a discernible upregulation in the expression of CCR2 and CXCR3 was observed (Fig. 7E and S6F). Histochemical analysis revealed a remarkable increase in the recruitment of macrophages around senescent hTICs in the livers of mice treated with PD-0332991 (Fig. 7F and S6G).

To elucidate immune system activation by senescent TICs, a flow cytometry-based multicolor analysis was conducted to identify differences in the proportion of immune cell populations within the livers of *Fah*$^{-/-}$ mice; for example, the identification of proportions from the C8 + P4 group and C12 group, including CD4$^+$ T cells (CD3$^+$CD4$^+$CD8$^-$), CD8$^+$ T cells (CD3$^+$CD4$^-$CD8$^+$), NK cells (CD49b$^+$), NKT cells (CD49b$^+$CD3$^+$), Treg cells (CD4$^+$Foxp3$^+$-CD3$^+$), and macrophages (CD11b$^+$F4/80$^+$). The analysis revealed a

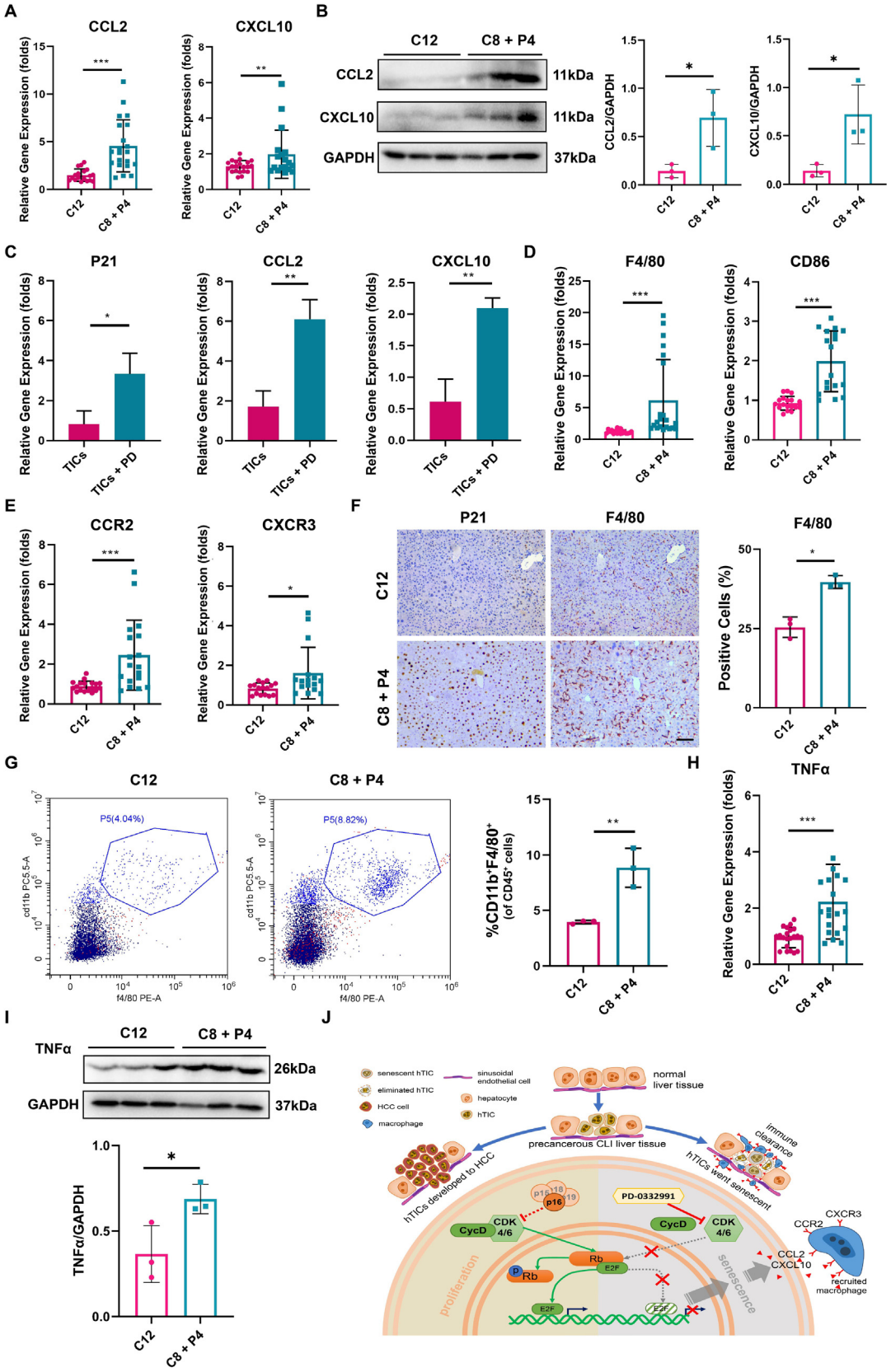
A
CCL2
CXCL10
Relative Gene Expression (folds)
C12
C8 + P4
B
C12
C8 + P4
CCL2
CXCL10
GAPDH
11kDa
11kDa
37kDa
CCL2/GAPDH
CXCL10/GAPDH
C
P21
CCL2
CXCL10
TICs
TICs + PD
D
F4/80
CD86
E
CCR2
CXCR3
F
P21
F4/80
C12
C8 + P4
Positive Cells (%)
G
C12
C8 + P4
P5(4.04%)
P5(8.82%)
cd11b PC5.5-A
f4/80 PE-A
%CD11b+F4/80+ (of CD45+ cells)
H
TNFα
I
TNFα
C12
C8 + P4
26kDa
GAPDH
37kDa
TNFα/GAPDH
J
senescent hTIC
eliminated hTIC
HCC cell
macrophage
sinusoidal endothelial cell
hepatocyte
hTIC
normal liver tissue
precancerous CLI liver tissue
hTICs developed to HCC
hTICs went senescent
Immune clearance
PD-0332991
CycD
CDK 4/6
Rb
E2F
proliferation
senescence
CCR2
CXCR3
CCL2
CXCL10
recruited macrophage

significant increase in the proportion of macrophages in adjacent non-tumor tissues of CLI mice treated with PD-0332991 compared to the control group (Fig. 7G). Intriguingly, the expression of tumor necrosis factor α (TNF-α), which is secreted by macrophages cells upon activation, was also significantly increased (Fig. 7H-I and S6H-I).

Collectively, these experimental findings suggest that CDK4/6 inhibitors effectively induce senescence of hTICs, contributing to the high expression of SASP factors CCL2 and CXCL10, which subsequently activate and recruit macrophages, foster antitumor immunity, and mitigate hepatocarcinogenesis (Fig. 7J).

Discussion

In this study, we investigated the effect of selectively inhibiting the Cyclin D-CDK4/6-INK4-Rb pathway on carcinogenesis leading to HCC by employing *Fah*$^{-/-}$ and N-Ras + AKT murine models to construct spontaneous HCC under CLI. To our knowledge, this is the first study to demonstrate that the CDK4/6 inhibitor PD-0332991 significantly reduces the incidence of HCC and attenuates the degree of liver injury in the precancerous stage of HCC, in these circumstances. Utilizing histochemical staining and *in vitro* isolation of hTICs, we validated the induction of cellular senescence in hTICs by PD-0332991, which inhibited HCC occurrence and promoted antitumor immunity under CLI. Our findings provide evidence supporting the viability of small-molecule drugs, specifically CDK4/6 inhibitors, as a feasible strategy against tumorigenesis via induction of hTICs senescence.

Hepatitis B virus (HBV) infection, alcoholic hepatitis, nonalcoholic hepatitis, and hepatitis C are the major causative factors of HCC [52]. These etiologies lead to long-term recurrent CLI that gradually progresses to hepatic fibrosis, cirrhosis, and ultimately HCC. At the hepatocellular level, CLI resulting from different disease backgrounds has several common characteristics, including inadequate blood perfusion, hypoxia, inflammatory environments, oxidative stress, endoplasmic reticulum stress, and exposure to mutagenic and mitotic factors [52,53]. To simulate the process of human chronic liver disease in HCC, we selected *Fah*$^{-/-}$ mice and N-Ras + AKT mice as animal models. Hepatocyte injury in *Fah*$^{-/-}$ mice is mainly characterized by genetic mutations, oxidative stress, and endoplasmic reticulum stress, whereas injury in N-Ras + AKT mice is mainly characterized by fat metabolism disorders. By using these two models, we aimed to increase the generalizability of the experimental results and make them more clinically relevant.

Excessive activation of the Cyclin D-CDK4/6-INK4-Rb signaling pathway correlates with uncontrolled cell proliferation, making it a promising target for small-molecule drugs. PD-0332991 is a highly specific small molecule that inhibits this pathway and its effect is dependent on the degree of activation of the Cyclin D-CDK4/6-INK4-Rb signaling pathway. In 2006, Lu and Schulze-Gahmenthe described the mechanism of PD-0332991 into the hinge region of CDK6, as well as the intermolecular hydrogen bonds that determine binding specificity**.** The semi-inhibitory concentrations of PD-0332991 for CDK4 and CDK6 were 9 ∼ 11 nmol/L and 15 nmol/L, respectively. In contrast, PD-0332991 demonstrated minimal or no inhibitory activity against 36 other protein kinases, including CDK2, CDK1, CDK5, and a variety of tyrosine, serine, and threonine kinases [54]. Moreover, except in tissues such as the bone marrow, normal adult cells are essentially in a quiescent state and unaffected by PD-0332991 [55]. PD-0332991 was approved by the FDA in 2015 and the China Food and Drug Administration (CFDA) in 2018 for the first-line treatment of ER^{+}/HER2^{-} breast cancer because of its clear pharmacological mechanism and high safety. Understanding the preventive effects of PD-0332991 on HCC occurrence may expand potential drug adaptations. Pre-malignant lesions, ranging from dysplastic foci to DN, are often observed in damaged and cirrhotic livers and are more proliferative than the surrounding parenchyma [56]. He *et al.* revealed that hTICs exist in these pre-malignant lesions and are involved in their maintenance and progression [36]. Therefore, patients with cirrhosis who have already developed DNs may get a better preventive effect.

In *Fah*$^{-/-}$ and N-Ras + AKT mice across different stages of CLI, only a fraction of hepatocytes was significantly positive for proliferation markers and susceptible to PD-0332991, suggesting a low probability of large-scale off-target effects during PD-0332991 medication. To further analyze the effect of PD-0332991 on the liver injury of mice under CLI, we measured serum alanine transaminase (ALT), aspartate aminotransferase (AST), albumin (ALB), and total bilirubin (TBIL) levels (Figures S1B, D). The results showed that PD-0332991 treatment in the precancerous stage did not exacerbate liver injury. However, the dosing cycle of PD-0332991 in animal experiments is shorter than the months to years required for human dosing. In general, PD-0332991 is less toxic and more reversible than other chemotherapeutic drugs, and the treatment process is safe and manageable.

In the chronic injured liver, hTICs are mainly derived from hepatocytes and play a dominant role in the progression of DN to HCC [57,58]. Here, we found that aberrant activation of the Cyclin D-CDK4/6-INK4-Rb signaling pathway was the main driving pathway within hTICs in both CLI models. In clinical patients, this pathway is highly activated in the precancerous stage, and the activation level is even higher than that in HCC. The results also demonstrated that PD-0332991 inhibited Rb phosphorylation and

Fig. 7. Senescent hTICs secreted SASP factors and thereby activating macrophages in the liver of *Fah*$^{-/-}$ mice with chronic liver injury. (A) RT-qPCR analysis of CCL2 and CXCL10 in the liver of *Fah*$^{-/-}$ mice in the C12 and the C8 + P4 groups; n = 5–7 mice/group. (Relative gene expression of CCL2 in C12 group: 1.50 ± 0.64 and C8 + P4 group: 4.55 ± 2.72; relative gene expression of CXCL10 in C12 group: 1.29 ± 0.33 and C8 + P4 group: 1.97 ± 1.35. All values are folds and shown in mean ± SD). (B) Immunoblot of the expression of CCL2 and CXCL10 in C12 group and C8 + P4 group, and statistical analysis of differences in expression. (C) RT-qPCR analysis of P21, CCL2 and CXCL10 in TICs, TICs + PD group cells after 48 h of *in vitro* culture; (Relative gene expression of P21 in TICs group: 0.82 ± 0.66 and TICs + PD group: 3.33 ± 1.04; relative gene expression of CCL2 in TICs group: 1.71 ± 0.79 and TICs + PD group: 6.10 ± 0.99. All values are folds and shown in mean ± SD). (D) RT-qPCR analysis of F4/80 and CD86 in the liver of *Fah*$^{-/-}$ mice in the C12 and the C8 + P4 groups; n = 5–7 mice/group. (Relative gene expression of F4/80 in C12 group: 1.20 ± 0.31 and C8 + P4 group: 6.17 ± 6.39; relative gene expression of CD86 in C12 group: 0.93 ± 0.17 and C8 + P4 group: 1.99 ± 0.77. All values are folds and shown in mean ± SD). (E) RT-qPCR analysis of CCR2 and CXCR3 in the liver of *Fah*$^{-/-}$ mice in the C12 and the C8 + P4 groups; n = 5–7 mice/group. (Relative gene expression of CCR2 in C12 group: 0.89 ± 0.26 and C8 + P4 group: 2.45 ± 1.76; relative gene expression of CXCR3 in C12 group: 0.82 ± 0.29 and C8 + P4 group: 1.61 ± 1.30. All values are folds and shown in mean ± SD). (F) IHC staining of macrophages (F4/80^{+}) in the livers of *Fah*$^{-/-}$ mice in the C12 and the C8 + P4 groups; and statistics analysis of proportion of positive cells. n = 3 mice/group. (G) Flow cytometry analysis of macrophages (CD11b^{+}F4/80^{+}) in adjacent non-tumor tissues from liver of *Fah*$^{-/-}$ mice in the C12 group and the C8 + P4 group, and the statistics of differences between them; n = 3 mice/group. (H) Quantitative expression analysis of TNF-α in the livers of *Fah*$^{-/-}$ mice in the C12 group versus the C8 + P4 group; n = 5–7 mice/group. (Relative gene expression of TNF-α in C12 group: 0.95 ± 0.35 and C8 + P4 group: 2.23 ± 1.33 folds. All values are folds and shown in mean ± SD). (I) Immunoblot of the expression of TNFα in C12 group and C8 + P4 group, and the relative expression analysis of the protein. (J) Pattern diagram of the HCC occurrence inhibition by PD-0332991 in this study. *, $p < 0.05$; **, $p < 0.01$; ***, $p < 0.001$.

induced senescence of hTICs in CLI mice; however, we could not completely exclude the effect of PD-0332991 on normally proliferating hepatocytes. In addition, the analysis of The Cancer Genome Atlas (TCGA) human data showed that 30 % of patients with HCC have a functional deletion of *RB1* [15], and this type of deletion is highly likely to lead to intrinsic resistance to PD-0332991 in precancerous patients carrying the mutation. Therefore, the sequencing analysis of patients is necessary before the application of PD-0332991. We also believe that precancerous patients with overactivation of the Cyclin D-CDK4/6-INK4-Rb signaling pathway would achieve the preferable preventive results with this drug.

Acquired resistance to PD-0332991 is also a matter of concern. Cyclin E-CDK2 may be responsible for excess phosphorylation of Rb, thus is involved in promoting cellular G1/S phase conversion and is one of the acquired multi-tumor resistance mechanisms to CDK4/6 inhibitors [59]. In breast cancer cells, acquired tumor resistance to PD-0332991 is restored by the combination of CDK2 and CDK4 inhibitors [60,61]. Activation of cell growth signaling pathways in genes such as *ESR1*, *FGFR2*, *ERBB3*, *MTOR*, and *MERTK* can also trigger tumor cell resistance to PD-0332991 [60,62]. To overcome acquired PD-0332991 resistance caused by these side-path activations, researchers are deploying two targets or even multiple targets to synchronize the inhibition of cell cycle pathways and abnormally activated growth or side pathways [40,61–63]. Given that patients with HCC usually progress from CLI diseases, the therapeutic efficacy of PD-0332991 after HCC may be affected by multiple cell cycle axes and side signaling pathways. PD-0332991 treatment at the stage of precancerous transformation to prevent HCC may have greater feasibility and therapeutic value than that after HCC.

According to previous studies, PD-0332991 affects the immune response by inhibiting the Cyclin D-CDK4/6-INK4-Rb signaling pathway. Suppression of CDK4/6-Rb signaling increases the expression of interferons and secretion of SASP-associated factors, which enhance the antigenicity of tumor cells [19,64]. Senescent pre-malignant hepatocytes can recruit and activate immune cells via their SASP factors, which clear senescent hepatocytes ('senescence surveillance'), thereby prevent HCC occurrence [9]. Using qPCR, we evaluated the expression changes of several SASP factors, including TGF-β, IL-1β, IL-6 and TNFα, in the liver tissues of CLI mice before and after PD-0332991 treatment. The evaluation revealed a significant reduction in the expression of TGF-β and IL-1β following PD-0332991 treatment (data not shown). Elevated expression of TGF-β and IL-1β is correlated with hepatic steatosis and hepatic fibrosis in several mouse models of liver disease or HCC [65,66]. The absence of hepatic fibrosis during CLI, and attenuation of hepatic steatosis after PD-0332991 treatment, were consistent with the downregulation of TGF-β and IL-1β in our two model mice.

Several factors of SASP are the substrates of ADAM17 (ADAM metallopeptidase domain 17, or TNFα converting enzyme, TACE), including EGFR, IL-6 and TNFα [67,68]. No significant change in ADAM17 expression was observed by us. It is reported that ADAM17 plays a pivotal role in liver regeneration, hepatic steatosis and hepatic fibrosis in mouse models of liver injury [69]. But liver regeneration capacity in our two models was inhibited, and no liver fibrosis was observed. Although, the N-Ras + AKT mice exhibited extensive hepatic steatosis, the *Fah*$^{-/-}$ mice displayed only mild hepatic steatosis. ADAM17 is primarily involved in the invasion and metastasis of HCC [70,71]. In our models, we focused on the pre-HCC stage. ADAM17-mediated IL6 activation is involved in neutrophil apoptosis, and ADAM17 expression and EGF-R activation exerts a protective effect on the liver by inhibiting apoptosis [72–74], all suggesting a strong correlation between ADAM17 and apoptosis in liver. In both of our models, apoptosis is inhibited and no positive cells were observed by TUNEL staining. Accordingly, we posit that the aforementioned factors collectively account for the absence of notable discrepancies in the expression levels of ADAM17, as well as IL-6 and EGF-R, in our experiments.

The factor responsible for the amplification of immunosuppressive iMC accumulation as well as myeloid cell-mediated senescent cell clearance was identified as CCL2, which has been reported to be a component of the SASP components [9,46,75] and functions as a chemokine to attract immune cells expressing the receptor CCR2 [76]. The CXCL10-CXCR3 axis also plays a positive role in macrophage infiltration [51]. These chemokines have been implicated in tumor inhibition during the early stages of tumor development [77,78]. Our investigation also highlighted that CDK4/6 inhibitor-induced senescent hTICs secrete the SASP factors, CCL2 and CXCL10, recruit macrophages, and activate immune responses to inhibit the occurrence of HCC.

Overall, CDK4/6-induced senescence of hTICs activated immune surveillance and restricted tumorigenesis in a CLI murine model, whereas prolonged use of PD-0332991 in the clinical setting suppressed immunocompetence, necessitating a 1-week break in the drug after every three weeks of oral administration [79]. In a murine model, the 4-week cycle of the entire experiment did not necessitate a break in administration, which would have a negative effect on the inhibition of HCC proliferation [15]. Further validation in subsequent experiments is required to determine whether the results of the murine model support an improved immune response to longer periods of medication.

Conclusion

We conducted a senescence-inducing treatment with a CDK4/6 inhibitor during HCC initiation in two murine models of CLI. Our findings revealed that the CDK4/6 inhibitor effectively prevented HCC occurrence by inducing the senescence of hTICs by inhibiting the Cyclin D-CDK4/6-INK4-Rb pathway. Moreover, the surveillance of hTICs for senescence is a limiting factor in the development of HCC. This study expands the clinical application potential of CDK4/6 inhibitors for the prevention of cirrhotic patients susceptible to HCC progression and provides valuable insights for clinical intervention strategies.

Materials and methods

Mice

Fah$^{-/-}$ mice of strain 129S4 and N-Ras + AKT mice of strain C57 BL/6J were used in this experiment. All mice were kept under specific pathogen free (SPF) conditions and animal experiments were conducted in accordance with the protocol approved by the Animal Care and Use Committee of Shanghai East Hospital. Mice were housed with a "light: dark" cycle of 12 h, ambient temperature of 24 °C, humidity of 55 %, and free access to water and food.

Chronic liver injury models and mouse drug administration

Modeling CLI in *Fah*$^{-/-}$ mice: To prevent the liver injury prior to the experiment, a blocking dose (7.5 mg/L, 100 %) of NTBC was added to the drinking water of *Fah*$^{-/-}$ mice. Male mice that reached the suitable weight (8-week-old, over 25 g) were randomly assigned to each group. After assignment, the drinking water of mice was replaced with sterile water containing a 187.5 μg/L dose (2.5 % of the blocking dose) of NTBC to induce CLI. All other conditions remained constant. Mice were weighed and their weight was recorded weekly. Finally, their serum and liver tissues were collected at the end of the experimental procedure in each group.

Fah$^{-/-}$ mice in Group C8 were given water containing the CLI-induction dose of NTBC for 8 weeks; *Fah*$^{-/-}$ mice in Group C12 were given water containing the CLI-induction dose of NTBC for 12 weeks; *Fah*$^{-/-}$ mice in Group C8 + P4 were given water containing the CLI-induction dose of NTBC for 12 weeks. But in the last 4 weeks, they also received daily gavage of PD-0332991 and were weighed daily, and small intestinal tissues were collected in addition to serum and liver tissues at the end of the experimental procedure.

Modeling CLI in N-Ras + AKT mice: Male mice that reached the suitable weight (8-week-old, over 25 g) were randomly assigned to each group. After assignment, a dilution containing 20 μg of pT3-myr-AKT-HA plasmids and 20 μg of pT/Caggs-NRASV12 plasmids, along with 1.6 μg of transposase pCMV (CAT) T7-SB100 in 2 mL of sterile saline was injected into the tail vein of C57BL/6 mice in 5–7 s. The combination of N-Ras + AKT proto-oncogenes plasmids led to tumor initiation approximately 4 weeks after tail vein injection, with 100 % tumor formation after 6 weeks [80]. Mice were weighed and their weight was recorded weekly. Finally, their serum and liver tissues were collected at the end of the experimental procedure in each group. All other conditions remained constant.

Group N-Ras + AKT: mice received no additional intervention, and tissue samples were collected after 6 weeks; Group N-Ras + AKT + PD: mice received no additional intervention during the first 2 weeks after plasmids injection. Starting from the third week, the mice received daily gavage of PD-0332991 and were weighed daily. Tissue samples were collected after 6 weeks. Information of the experimental regents is detailed in Supplementary Table 3.

Isolation and culture of hepatic tumor-initiating cells

Hepatocytes were obtained by *in situ* collagenase perfusion of the livers from C8 group *Fah*$^{-/-}$ mice and N-Ras + AKT group mice. The harvested cells were filtered first through a 70 μm filter and then through a 40 μm filter. The collagenase-resistant hyperplasia hepatocytes (pre-cancerous cells) are obtained from the upper layer of the 40 μm filter, as they were aggregated as clusters. The obtained aggregated TICs and non-aggregated hepatocytes were spread on collagen-coated culture dishes at a density of 2×10^4 cells per square centimeter.

The cell culture medium was prepared by mixing 20 % heat-inactivated fetal bovine serum, 0.01 g/L insulin, 1 μM dexamethasone, 1 % glutamine, 20 μg/L EGF, and 1 × antibiotic antifungal into Dulbecco's Modified Eagle Medium containing 4.5 g/L glucose [37]. Information of the experimental regents is detailed in Supplementary Table 3.

Hematoxylin eosin staining, immunohistochemical staining, serum indicators

For the H&E staining, the fresh liver tissues were fixed in 4 % paraformaldehyde for 48 h, followed by dehydration, dealcoholization and paraffin embedding. Embedded tissues were sliced into 2 μm sections. After baking, dewaxing, and rehydration, the sections were stained by hematoxylin for 5–10 min, rinsed, stained with eosin, dehydrated, and sealed with neutral resin.

For the immunohistochemical (IHC) staining, the fresh liver tissues were treated in the same protocol as those for H&E staining before rehydration. The sections were then soaked in 0.01 M citric acid buffer (pH 6.0) or EDTA (Ethylenediaminetetraacetic acid, pH 9.0) and sterilized in a pressure cooker for 2–4 min at 121℃/100 kPa. Once cooled to room temperature, endogenous peroxidases on the sections were blocked with 3 % H_2O_2 solution, and 1 % bovine serum albumin was used to block antibodies' non-specific binding sites on the sections for 30 min at room temperature. The sections were then incubated with the primary antibodies at 4℃ overnight and HRP-conjugated secondary antibodies at 37℃ for 30 min. DAB staining was applied, followed by staining with haematoxylin. The sections were then rapidly dehydrated and mounted with neutral resin.

For serum biochemical analysis, blood samples were collected from the *retro*-orbital venous sinus of mice. The samples were then centrifuged at 3000 g for 15 min, and stored at −80℃. Serum biochemical analysis followed a predefined protocol [21]. Antibodies and experimental regents are listed in Supplementary Table 1 and Supplementary Table 3, respectively.

Cellular immunofluorescence

The cell culture medium was discarded, and dishes were washed with PBS. Cultured cells in dishes were fixed with 4 % PFA for 15 min at room temperature. Next, the cell membranes were permeabilized with 0.25 % TritonX-100 for 15 min, followed by rinsing with PBS. To deplete endogenous peroxidase, cells were incubated with 0.3 % H_2O_2 in the dark for 15 min. To block non-specific binding sites of antibodies, cells were incubated with 10 % goat serum (containing 0.3 M glycine) for 40 min at room temperature. Cells were incubated with primary antibodies overnight at 4℃. Then fluorescent secondary antibody were added to cells and incubated at 37℃ in the dark for 30 min. The cells were then stained with 1 × DAPI for 5 min and washed with PBS. The antibodies are detailed in Supplementary Table 1. The immunofluorescence co-staining protocol remains the same, except that during the incubation process, the primary antibodies used are from different species.

Senescence associated-β-galactosidase assay

Mouse liver tissues, upon acquisition, were promptly sectioned into appropriate sizes, immersed in OCT, and rapidly cooled to −80℃ for storage. After restoring tissue temperature on a frozen sectioning machine, tissues in OCT were sliced into 5 μm frozen sections. Sections were washed thrice with PBS to remove OCT, followed by fixation in SA-β-Gal solution at room temperature for 5 min and PBS rinse. Subsequently, sections were treated with SA-β-Gal staining solution, incubated at 37℃ overnight. Experimental kit details are provided in Supplementary Table 3. For fluorescence staining of SA-β-Gal, all assays follow the protocols of the SPiDER-β-Gal staining kit (Dojindo, SG03).

Immunoblotting assay

To obtain sufficient TICs for WB experiments, TICs are generally obtained after *in vitro* expansions. The cells and tissues were lysed using RIPA buffer supplemented with a protease inhibitor cocktail. The protein samples were then resolved using SDS-PAGE and transferred to PVDF membranes (Millipore, no. ISEQ00010). After blocking the membranes with 5 % skimmed milk (in TBST) for 1 h at room temperature, they were incubated with the primary antibody overnight at 4°C. Subsequently, the membranes were incubated with the HRP-conjugated IgG at room temperature for 1 h. Finally, the bands were visualized using enhanced chemiluminescence. Antibodies used are listed in Supplementary Table 1. Reagents information is provided in Supplementary Table 3.

Real-time quantitative polymerase chain reactions analysis

Total RNA was extracted using the extraction Kit and reverse-transcribed using SuperScript™ II Reverse Transcriptase following the manufacture's guidelines. PCR and real-time quantitative PCR

(RT-qPCR) were performed. The primers and conditions are listed in Supplementary Table 2.

Flow cytometry analysis

Mouse livers were harvested, rinsed with saline or DMEM, and minced on a Petri dish. Digestion was carried out using 4.2 mL of Mouse Liver Dissociation Kit (Miltenyi, 130–105-807) at 37℃/150 rpm for 30 min. After digestion, the suspension was filtered through a 70 μm filter, rinsed with DMEM, and centrifuged. The resulting cell precipitate underwent Percoll density gradient centrifugation, followed by washing and resuspension in 1 % inactivated fetal bovine serum. Immune cells were obtained from the liver tissues.

The cell precipitate was resuspended in stain buffer, treated with fc block, and then stained with Flow Cytometry antibody. Live/dead dye was added, and the reaction was terminated with PBS. After centrifugation, the precipitate was resuspended in stain buffer and incubated with Flow Cytometry antibody. If the antigen is located in the nucleus, a membrane rupture was performed before antibody staining. Afterward, the final suspension was prepared for Flow Cytometry Analysis.

For the isolation process, the Percoll stock solution was diluted with 10 × PBS to obtain 35 % Percoll. Antibodies used are detailed in Supplementary Table 1.

Data collection and analysis

The RNA-seq dataset GSE148355 was obtained from the publicly available Gene Expression Omnibus (GEO) database. The dataset includes non-tumor samples, precancerous samples with different degrees of fibrosis and HCC samples from the Seoul National University Hospital in Korea between 2004 and 2009. For our analysis, the normalized data (FPKM) of these precancerous and tumor samples were used, including 15 non-tumor control samples (Normal), 10 samples with a low degree of fibrosis (Fibrosis low, FL), 10 samples with a high degree of fibrosis (Fibrosis high, FH), 10 samples with cirrhosis (Cirrhosis, CS), 10 samples with low degree dysplastic nodule (Dysplastic nodule low, DL), 7 samples with high degree dysplastic nodule (Dysplastic nodule high, DH), 10 samples with tumor grade1 (TG1, estimated by the Edmonson and Steiner classification), 25 samples with tumor grade2 (TG2, estimated by the Edmonson and Steiner classification) and 19 samples with tumor grade3 (TG3, estimated by the Edmonson and Steiner classification).

To inspect how the Cyclin D-CDK4/6-INK4-Rb signaling pathway activated in patients at various stages of precancerous liver, the algorithm ssGSEA in the GSVA R-package was applied to calculate the enrichment scores of above gene set in samples at different stages of precancerous development. The marker genes in the Cyclin D-CDK4/6-INK4-Rb pathway, mainly including *CDK4*, *CDK6*, *CDK2*, *RB1*, *CCND1*, *CDKN2A*, and *CDKN1A* were customized as a functional gene set for calculating the pathway score. The pathway enrichment scores of normal group and different disease groups were analyzed by Wilcoxon rank sum test; *, $p < 0.05$; **, $p < 0.01$; ***, $p < 0.001$.

RNA sequencing and bioinformatics analysis

Two liver samples from mice in group C0, three from mice in group C8, two from mice in group C12, and three from mice in group C8 + P4 were sent to bulk RNA-seq service of Shanghai OE Biotech Co. The sequencing reads were mapped to the reference genome using hisat2.56, and FPKM values for each gene expression were counted using Cufflinks. Intergroup differential gene expression analysis was performed using DESeq2, and then volcano maps of differentially up- and down-regulated genes were plotted using ggplot2, and the differentially expressed genes were screening with a criterion of absolute Fold Change > 2 and adjusted *P* value < 0.05. Gene expression heatmaps were plotted using the pheatmap package. Temporal trend analysis of gene expression and delineation of clustered gene clusters with different expression patterns were performed using the R package Mfuzz. GO and KEGG gene enrichment analyses were performed using the ClusterProfiler package to focus on the function of differential expression genes.

Statistical analysis

Immunoblots were quantified in grayscale using ImageJ 1.53a, with data expressed as mean ± standard deviation (S.D.). Tumor incidence rates were analyzed using Fisher's exact test. For data not conforming to a normal distribution, the sign rank sum test was employed. Data conforming to a normal distribution were analyzed using the Student *t*-test or one-way analysis of variance (ANOVA). Graphs and statistical analyses were performed using GraphPad Prism 8.4. All experiments included at least three biological replicates. Statistical significance was determined with *p* values, where values greater than 0.05 were considered not significant (ns), and significance levels were denoted as follows: $^{*}p < 0.05$, $^{**}p < 0.01$, $^{***}p < 0.001$.

Declaration of competing interest

The authors declare that they have no known competing financial interests or personal relationships that could have appeared to influence the work reported in this paper.

Acknowledgements

Authors were grateful to Xicheng Wang, Xiaolan Mu and Jialing Wu for their kindly assistance and meaningful discussion during manuscript preparation. Authors also thanks to Dr. Liang Zheng (Shanghai East Hospital, Tongji University, China) for giving advice on statistics. This work was funded by the Major Program of National Key Research and Development Project (2019YFA0801502, 2020YFA0112600), National Natural Science Foundation of China (82173019, 82270638, 82203741, 82300718), the Project of Shanghai Science and Technology Commission (22ZR1451100, 22Y11908500), Jiangxi Provincial Natural Science Foundation (20212ACB206033), Shanghai Engineering Research Center of Stem Cells Translational Medicine (20DZ2255100), and Peak Disciplines (Type IV) of Institutions of Higher Learning in Shanghai.

Appendix A. Supplementary data

Supplementary data to this article can be found online at https://doi.org/10.1016/j.jare.2024.08.034.

References

[1] Bray F, Laversanne M, Sung H, Ferlay J, Siegel RL, Soerjomataram I et al. Global cancer statistics 2022: GLOBOCAN estimates of incidence and mortality worldwide for 36 cancers in 185 countries. CA Cancer J Clin 2024, 74 (3):229-263.

[2] Global Burden of Disease Liver Cancer C, Akinyemiju T, Abera S, Ahmed M, Alam N, Alemayohu MA, Allen C, Al-Raddadi R, Alvis-Guzman N, Amoako Y *et al*: The Burden of Primary Liver Cancer and Underlying Etiologies From 1990 to 2015 at the Global, Regional, and National Level: Results From the Global Burden of Disease Study 2015. *JAMA Oncol* 2017, 3(12):1683-1691.

[3] Paik JM, Golabi P, Younossi Y, Mishra A, Younossi ZM. Changes in the Global Burden of Chronic Liver Diseases From 2012 to 2017: the Growing Impact of NAFLD. Hepatology 2020;72(5):1605–16.

[4] Chen R, Nishimura MC, Bumbaca SM, Kharbanda S, Forrest WF, Kasman IM, et al. A hierarchy of self-renewing tumor-initiating cell types in glioblastoma. Cancer Cell 2010;17(4):362–75.
[5] Ma Y, Yang X, Zhao W, Yang Y, Zhang Z. Calcium channel alpha2delta1 subunit is a functional marker and therapeutic target for tumor-initiating cells in non-small cell lung cancer. Cell Death Dis 2021;12(3):257.
[6] Bansal N, Bartucci M, Yusuff S, Davis S, Flaherty K, Huselid E, et al. BMI-1 targeting interferes with patient-derived tumor-initiating cell survival and tumor growth in prostate cancer. Clin Cancer Res 2016;22(24):6176–91.
[7] Serrano M, Lin AW, McCurrach ME, Beach D, Lowe SW. Oncogenic ras provokes premature cell senescence associated with accumulation of p53 and p16INK4a. Cell 1997;88(5):593–602.
[8] Lopez-Otin C, Blasco MA, Partridge L, Serrano M, Kroemer G. Hallmarks of aging: an expanding universe. Cell 2023;186(2):243–78.
[9] Kang TW, Yevsa T, Woller N, Hoenicke L, Wuestefeld T, Dauch D, et al. Senescence surveillance of pre-malignant hepatocytes limits liver cancer development. Nature 2011;479(7374):547–51.
[10] Wang C, Vegna S, Jin H, Benedict B, Lieftink C, Ramirez C, et al. Inducing and exploiting vulnerabilities for the treatment of liver cancer. Nature 2019;574(7777):268–72.
[11] Sherr CJ, Roberts JM. CDK inhibitors: positive and negative regulators of G1-phase progression. Genes Dev 1999;13(12):1501–12.
[12] Wang B, Varela-Eirin M, Brandenburg SM, Hernandez-Segura A, van Vliet T, Jongbloed EM, et al. Pharmacological CDK4/6 inhibition reveals a p53-dependent senescent state with restricted toxicity. EMBO J 2022;41(6):e108946.
[13] Knudsen ES, Kumarasamy V, Nambiar R, Pearson JD, Vail P, Rosenheck H, et al. CDK/cyclin dependencies define extreme cancer cell-cycle heterogeneity and collateral vulnerabilities. Cell Rep 2022;38(9):110448.
[14] Goel S, DeCristo MJ, McAllister SS, Zhao JJ. CDK4/6 inhibition in cancer: beyond cell cycle arrest. Trends Cell Biol 2018;28(11):911–25.
[15] Bollard J, Miguela V, Ruiz de Galarreta M, Venkatesh A, Bian CB, Roberto MP, et al. Nguyen CB *et al.*: palbociclib (PD-0332991), a selective CDK4/6 inhibitor, restricts tumour growth in preclinical models of hepatocellular carcinoma. Gut 2017;66(7):1286–96.
[16] Vigano L, Locatelli A, Ulisse A, Galbardi B, Dugo M, Tosi D, et al. Modulation of the estrogen/erbB2 receptors cross-talk by CDK4/6 inhibition triggers sustained senescence in estrogen receptor- and ErbB2-positive breast cancer. Clin Cancer Res 2022;28(10):2167–79.
[17] Turner NC, Ro J, Andre F, Loi S, Verma S, Iwata H, et al. Palbociclib in hormone-receptor-positive advanced breast cancer. N Engl J Med 2015;373(3):209–19.
[18] Finn RS, Martin M, Rugo HS, Jones S, Im SA, Gelmon K, et al. Palbociclib and letrozole in advanced breast cancer. N Engl J Med 2016;375(20):1925–36.
[19] Ruscetti M, Leibold J, Bott MJ, Fennell M, Kulick A, Salgado NR, et al. NK cell-mediated cytotoxicity contributes to tumor control by a cytostatic drug combination. Science 2018;362(6421):1416–22.
[20] Klein ME, Kovatcheva M, Davis LE, Tap WD, Koff A. CDK4/6 inhibitors: the mechanism of action may not be as simple as once thought. Cancer Cell 2018;34(1):9–20.
[21] Wang C, Chen WJ, Wu YF, You P, Zheng SY, Liu CC, et al. The extent of liver injury determines hepatocyte fate toward senescence or cancer. Cell Death Dis 2018;9(5):575.
[22] Grompe M, al-Dhalimy M, Finegold M, Ou CN, Burlingame T, Kennaway NG, Soriano P: Loss of fumarylacetoacetate hydrolase is responsible for the neonatal hepatic dysfunction phenotype of lethal albino mice. *Genes Dev* 1993, 7(12A):2298-2307.
[23] Lindstedt S, Holme E, Lock EA, Hjalmarson O, Strandvik B. Treatment of hereditary tyrosinaemia type I by inhibition of 4-hydroxyphenylpyruvate dioxygenase. Lancet 1992;340(8823):813–7.
[24] Willenbring H, Sharma AD, Vogel A, Lee AY, Rothfuss A, Wang Z, et al. Loss of p21 permits carcinogenesis from chronically damaged liver and kidney epithelial cells despite unchecked apoptosis. Cancer Cell 2008;14(1):59–67.
[25] Buitrago-Molina LE, Marhenke S, Longerich T, Sharma AD, Boukouris AE, Geffers R, et al. The degree of liver injury determines the role of p21 in liver regeneration and hepatocarcinogenesis in mice. Hepatology 2013;58(3):1143–52.
[26] Beier F, Martinez P, Blasco MA. Chronic replicative stress induced by CCl4 in TRF1 knockout mice recapitulates the origin of large liver cell changes. J Hepatol 2015;63(2):446–55.
[27] Ho C, Wang C, Mattu S, Destefanis G, Ladu S, Delogu S, et al. AKT (v-akt murine thymoma viral oncogene homolog 1) and N-Ras (neuroblastoma ras viral oncogene homolog) coactivation in the mouse liver promotes rapid carcinogenesis by way of mTOR (mammalian target of rapamycin complex 1), FOXM1 (forkhead box M1)/SKP2, and c-Myc pathways. Hepatology 2012;55(3):833–45.
[28] Krenning L, Feringa FM, Shaltiel IA, van den Berg J, Medema RH. Transient activation of p53 in G2 phase is sufficient to induce senescence. Mol Cell 2014;55(1):59–72.
[29] Macip S, Igarashi M, Fang L, Chen A, Pan ZQ, Lee SW, et al. Inhibition of p21-mediated ROS accumulation can rescue p21-induced senescence. EMBO J 2002;21(9):2180–8.
[30] Thangavel C, Boopathi E, Liu Y, McNair C, Haber A, Perepelyuk M, et al. Therapeutic challenge with a CDK 4/6 inhibitor induces an RB-dependent SMAC-mediated apoptotic response in non-small cell lung cancer. Clin Cancer Res 2018;24(6):1402–14.
[31] Li X, Seebacher NA, Garbutt C, Ma H, Gao P, Xiao T, et al. Inhibition of cyclin-dependent kinase 4 as a potential therapeutic strategy for treatment of synovial sarcoma. Cell Death Dis 2018;9(5):446.
[32] Malato Y, Naqvi S, Schurmann N, Ng R, Wang B, Zape J, et al. Fate tracing of mature hepatocytes in mouse liver homeostasis and regeneration. J Clin Invest 2011;121(12):4850–60.
[33] Itoh T, Miyajima A. Liver regeneration by stem/progenitor cells. Hepatology 2014;59(4):1617–26.
[34] Lei Y, Wang S, Liu J, Yan W, Han P, Tian D. Identification of MCM family as potential therapeutic and prognostic targets for hepatocellular carcinoma based on bioinformatics and experiments. Life Sci 2021;272:119227.
[35] Meagher M, Epling LB, Enemark EJ. DNA translocation mechanism of the MCM complex and implications for replication initiation. Nat Commun 2019;10(1):3117.
[36] He G, Dhar D, Nakagawa H, Font-Burgada J, Ogata H, Jiang Y, et al. Identification of liver cancer progenitors whose malignant progression depends on autocrine IL-6 signaling. Cell 2013;155(2):384–96.
[37] Zhang J, Han C, Ungerleider N, Chen W, Song K, Wang Y, et al. A transforming growth factor-beta and H19 signaling axis in tumor-initiating hepatocytes that regulates hepatic carcinogenesis. Hepatology 2019;69(4):1549–63.
[38] Dang DT, Chen F, Kohli M, Rago C, Cummins JM, Dang LH. Glutathione S-transferase pi1 promotes tumorigenicity in HCT116 human colon cancer cells. Cancer Res 2005;65(20):9485–94.
[39] Andersen JB, Loi R, Perra A, Factor VM, Ledda-Columbano GM, Columbano A, et al. Progenitor-derived hepatocellular carcinoma model in the rat. Hepatology 2010;51(4):1401–9.
[40] Sheng J, Kohno S, Okada N, Okahashi N, Teranishi K, Matsuda F, et al. Treatment of retinoblastoma 1-intact hepatocellular carcinoma with cyclin-dependent kinase 4/6 inhibitor combination therapy. Hepatology 2021;74(4):1971–93.
[41] Hamilton E, Infante JR. Targeting CDK4/6 in patients with cancer. Cancer Treat Rev 2016;45:129–38.
[42] Jee BA, Choi JH, Rhee H, Yoon S, Kwon SM, Nahm JH, et al. Dynamics of genomic, epigenomic, and transcriptomic aberrations during stepwise hepatocarcinogenesis. Cancer Res 2019;79(21):5500–12.
[43] Hernandez-Meza G, von Felden J, Gonzalez-Kozlova EE, Garcia-Lezana T, Peix J, Portela A, et al. DNA methylation profiling of human hepatocarcinogenesis. Hepatology 2021;74(1):183–99.
[44] Cheng N, Ren Y, Zhou J, Zhang Y, Wang D, Zhang X, et al. Deep learning-based classification of hepatocellular nodular lesions on whole-slide histopathologic images. Gastroenterology 2022;162(7):1948–1961 e1947.
[45] Kumar L. M EF: Mfuzz: a software package for soft clustering of microarray data. Bioinformation 2007;2(1):5–7.
[46] Acosta JC, Banito A, Wuestefeld T, Georgilis A, Janich P, Morton JP, et al. A complex secretory program orchestrated by the inflammasome controls paracrine senescence. Nat Cell Biol 2013;15(8):978–90.
[47] Kuilman T, Michaloglou C, Mooi WJ, Peeper DS. The essence of senescence. Genes Dev 2010;24(22):2463–79.
[48] Eggert T, Wolter K, Ji J, Ma C, Yevsa T, Klotz S, et al. Distinct functions of senescence-associated immune responses in liver tumor surveillance and tumor progression. Cancer Cell 2016;30(4):533–47.
[49] Chibaya L, Murphy KC, DeMarco KD, Gopalan S, Liu H, Parikh CN, et al. Morris JPt *et al.*: EZH2 inhibition remodels the inflammatory senescence-associated secretory phenotype to potentiate pancreatic cancer immune surveillance. *Nat*. Cancer 2023;4(6):872–92.
[50] Liu N, Wang X, Steer CJ, Song G. MicroRNA-206 promotes the recruitment of CD8(+) T cells by driving M1 polarisation of Kupffer cells. Gut 2022;71(8):1642–55.
[51] House IG, Savas P, Lai J, Chen AXY, Oliver AJ, Teo ZL, et al. Macrophage-derived CXCL9 and CXCL10 are required for antitumor immune responses following immune checkpoint blockade. Clin Cancer Res 2020;26(2):487–504.
[52] Toh MR, Wong EYT, Wong SH, Ng AWT, Loo LH, Chow PK, et al. Global epidemiology and genetics of hepatocellular carcinoma. Gastroenterology 2023;164(5):766–82.
[53] Berasain C, Arechederra M, Argemi J, Fernandez-Barrena MG, Avila MA. Loss of liver function in chronic liver disease: An identity crisis. J Hepatol 2023;78(2):401–14.
[54] Lu H, Schulze-Gahmen U. Toward understanding the structural basis of cyclin-dependent kinase 6 specific inhibition. J Med Chem 2006;49(13):3826–31.
[55] Hu W, Sung T, Jessen BA, Thibault S, Finkelstein MB, Khan NK, et al. Mechanistic investigation of bone marrow suppression associated with palbociclib and its differentiation from cytotoxic chemotherapies. Clin Cancer Res 2016;22(8):2000–8.
[56] Hytiroglou P, Park YN, Krinsky G, Theise ND: Hepatic precancerous lesions and small hepatocellular carcinoma. *Gastroenterol Clin North Am* 2007, 36(4):867-887, vii.
[57] Mu X, Espanol-Suner R, Mederacke I, Affo S, Manco R, Sempoux C, et al. Hepatocellular carcinoma originates from hepatocytes and not from the progenitor/biliary compartment. J Clin Invest 2015;125(10):3891–903.
[58] Tummala KS, Brandt M, Teijeiro A, Grana O, Schwabe RF, Perna C, et al. Hepatocellular carcinomas originate predominantly from hepatocytes and benign lesions from hepatic progenitor cells. Cell Rep 2017;19(3):584–600.
[59] Gladden AB, Diehl JA. Cell cycle progression without cyclin E/CDK2: breaking down the walls of dogma. Cancer Cell 2003;4(3):160–2.

[60] Formisano L, Lu Y, Servetto A, Hanker AB, Jansen VM, Bauer JA, et al. Aberrant FGFR signaling mediates resistance to CDK4/6 inhibitors in ER+ breast cancer. Nat Commun 2019;10(1):1373.
[61] Joshi JJ, Coffey H, Corcoran E, Tsai J, Huang CL, Ichikawa K, et al. H3B–6527 is a potent and selective inhibitor of FGFR4 in FGF19-driven hepatocellular carcinoma. Cancer Res 2017;77(24):6999–7013.
[62] Olmez I, Zhang Y, Manigat L, Benamar M, Brenneman B, Nakano I, et al. Combined c-Met/Trk inhibition overcomes resistance to CDK4/6 inhibitors in glioblastoma. Cancer Res 2018;78(15):4360–9.
[63] Heilmann AM, Perera RM, Ecker V, Nicolay BN, Bardeesy N, Benes CH, et al. CDK4/6 and IGF1 receptor inhibitors synergize to suppress the growth of p16INK4A-deficient pancreatic cancers. Cancer Res 2014;74(14):3947–58.
[64] Goel S, DeCristo MJ, Watt AC, BrinJones H, Sceneay J, Li BB, et al. CDK4/6 inhibition triggers anti-tumour immunity. Nature 2017;548(7668):471–5.
[65] Fan W, Liu T, Chen W, Hammad S, Longerich T, Hausser I, et al. ECM1 prevents activation of transforming growth factor beta, hepatic stellate cells, and fibrogenesis in mice. Gastroenterology 2019;157(5):1352–1367 e1313.
[66] Desert R, Chen W, Ge X, Viel R, Han H, Athavale D, et al. Hepatocellular carcinomas, exhibiting intratumor fibrosis, express cancer-specific extracellular matrix remodeling and WNT/TGFB signatures, associated with poor outcome. Hepatology 2023;78(3):741–57.
[67] Zunke F, Rose-John S. The shedding protease ADAM17: physiology and pathophysiology. *Biochim Biophys Acta Mol.* Cell Res 2017. 1864(11 Pt B):2059–2070.
[68] Mullberg J, Schooltink H, Stoyan T, Gunther M, Graeve L, Buse G, et al. The soluble interleukin-6 receptor is generated by shedding. Eur J Immunol 1993;23(2):473–80.
[69] Cai B, Dongiovanni P, Corey KE, Wang X, Shmarakov IO, Zheng Z, et al. Chung RT *et al.*: macrophage MerTK promotes liver fibrosis in nonalcoholic steatohepatitis. Cell Metab 2020;31(2):406–421 e407.
[70] Hong SW, Hur W, Choi JE, Kim JH, Hwang D, Yoon SK. Role of ADAM17 in invasion and migration of CD133-expressing liver cancer stem cells after irradiation. Oncotarget 2016;7(17):23482–97.
[71] Ding T, Yu Y, Gao L, Xiang L, Xu B, Gu B, et al. Predictive roles of ADAM17 in patient survival and immune cell infiltration in hepatocellular carcinoma. Int J Mol Sci 2023;24(23).
[72] Murthy A, Defamie V, Smookler DS, Di Grappa MA, Horiuchi K, Federici M, et al. Ectodomain shedding of EGFR ligands and TNFR1 dictates hepatocyte apoptosis during fulminant hepatitis in mice. J Clin Invest 2010;120(8):2731–44.
[73] Chalaris A, Rabe B, Paliga K, Lange H, Laskay T, Fielding CA, et al. Apoptosis is a natural stimulus of IL6R shedding and contributes to the proinflammatory trans-signaling function of neutrophils. Blood 2007;110(6):1748–55.
[74] Li Y, Brazzell J, Herrera A, Walcheck B. ADAM17 deficiency by mature neutrophils has differential effects on L-selectin shedding. Blood 2006;108(7):2275–9.
[75] Toso A, Revandkar A, Di Mitri D, Guccini I, Proietti M, Sarti M, et al. Enhancing chemotherapy efficacy in Pten-deficient prostate tumors by activating the senescence-associated antitumor immunity. Cell Rep 2014;9(1):75–89.
[76] Deshmane SL, Kremlev S, Amini S, Sawaya BE. Monocyte chemoattractant protein-1 (MCP-1): an overview. J Interferon Cytokine Res 2009;29(6):313–26.
[77] Qian BZ, Li J, Zhang H, Kitamura T, Zhang J, Campion LR, et al. CCL2 recruits inflammatory monocytes to facilitate breast-tumour metastasis. Nature 2011;475(7355):222–5.
[78] Schneider C, Teufel A, Yevsa T, Staib F, Hohmeyer A, Walenda G, et al. Adaptive immunity suppresses formation and progression of diethylnitrosamine-induced liver cancer. Gut 2012;61(12):1733–43.
[79] Flaherty KT, Lorusso PM, Demichele A, Abramson VG, Courtney R, Randolph SS, et al. Phase I, dose-escalation trial of the oral cyclin-dependent kinase 4/6 inhibitor PD 0332991, administered using a 21-day schedule in patients with advanced cancer. Clin Cancer Res 2012;18(2):568–76.
[80] Zhou L, Yu KH, Wong TL, Zhang Z, Chan CH, Loong JH, et al. Lineage tracing and single-cell analysis reveal proliferative Prom1+ tumour-propagating cells and their dynamic cellular transition during liver cancer progression. Gut 2022;71(8):1656–68.